Published in final edited form as:

Magn Reson Imaging Clin N Am. 2016 February ; 24(1): 157–186. doi:10.1016/j.mric.2015.08.005.

Multiparametric MR Imaging in Abdominal Malignancies

Antonio Luna, MD[a,b,*], **Shivani Pahwa, MD**[b], **Claudio Bonini, MD**[c], **Lidia Alcalá-Mata, MD**[a], **Katherine L. Wright, PhD**[b], and **Vikas Gulani, MD, PhD**[d,e,f]

[a]Department of Radiology, Health Time, Carmelo Torres 2, Jaén 23006, Spain

[b]Department of Radiology, University Hospitals of Cleveland, Case Western Reserve University, Cleveland, OH, USA

[c]Oroño Medical Diagnostic Center, Rosario, Argentina

[d]Department of Radiology, Case Comprehensive Cancer Center, University Hospitals of Cleveland, Case Western Reserve University, Cleveland, OH, USA

[e]Department of Urology, Case Comprehensive Cancer Center, University Hospitals of Cleveland, Case Western Reserve University, Cleveland, OH, USA

[f]Department of Biomedical Engineering, Case Comprehensive Cancer Center, University Hospitals of Cleveland, Case Western Reserve University, Cleveland, OH, USA

Keywords

MR imaging; DWI; Perfusion MR imaging; MR elastography; ^{1}H-MR spectroscopy; Hepatobiliary contrast agents; Multiparametric; Biomarker

INTRODUCTION

Anatomic MR imaging is the most sensitive imaging tool in the detection of hepatobiliary and pancreatic (HBP) malignancies.[1] The combination of morphologic features and enhancement patterns provides an integral assessment of these tumors, including therapy monitoring using size criteria.[2] Recently, new MR imaging techniques are able to explore functional and molecular characteristics of abdominal cancers (Table 1). This functional information is very useful for overcoming limitations of morphologic MR imaging and has shown particular promise in the assessment of therapy response to novel targeted therapies.[3] These techniques are inherently quantitative and yield absolute or relative measurements of tissue properties, providing potential imaging biomarkers of disease severity.[4–7]

This review focuses on basic concepts behind these techniques, clinical applications, and levels of validation in the analysis of abdominal malignancies, and also the integration of these technologies into a multiparametric imaging (MPI) approach.

*Corresponding author. aluna70@htime.org.

DIFFUSION-WEIGHTED MR IMAGING

Diffusion-weighted imaging (DWI) has gained ground in the upper abdomen, being included in state-of-the-art MR imaging protocols. This technique is easy to perform, relatively fast, and does not require administration of an extrinsic contrast agent. Its use facilitates lesion detection and characterization in the liver and pancreas. Furthermore, its role as a cancer biomarker of tissue cellularity and cell membrane integrity has been confirmed for HBP malignancies.[5]

DWI reflects the microscopic movement of water protons in different tissues. The net motion of water molecules is directly related to the movement of water in various tissue compartments. The presence of a dense cellular structure, many intact cell membranes, or viscous fluid with viscous content can reduce or restrict water mobility, which results in high signal on high b-value (heavily diffusion weighted) imaging and corresponds to low diffusivity on apparent diffusion coefficient (ADC) maps. Conversely, tissues with low cellularity show an increase in water diffusion, low signal intensity (SI) on high b-value images, and high diffusivity on ADC maps.

Technical Aspects of Diffusion-Weighted Imaging

Sequence design—An adequate sequence design of diffusion-weighted sequence in the upper abdomen is critical, because it has intrinsically limited spatial resolution. Box 1 summarizes the list of scanning parameters to be optimized in a DWI sequence of the body. Most commonly, a single-shot spin-echo echo-planar imaging sequence is performed, which has the advantage of a very fast readout, making it insensitive to macroscopic patient motion.[4] However, this family of sequences is prone to motion and magnetic susceptibility artifacts. The maintenance of echo time (TE) as short as possible, using parallel imaging, high bandwidth, and advanced suppression techniques, minimizes distortion artifacts, although diffusion requires intrinsically long TEs due to the time required to impart sufficient diffusion sensitivity. In order to reduce the effects of respiratory and cardiac motion, it is necessary to use gated acquisitions (Fig. 1). Most commonly, breath-hold or free-breathing sequences are used (Box 2). In addition, fat suppression must be used to avoid ghosting artifacts from the fat signal.

Modeling of diffusion signal—In order to use DWI as an oncological biomarker, quantitative mapping is critical, especially in the setting of therapy monitoring. The most widely used quantitative property is the ADC from a monocompartmental model of diffusion signal decay. ADC measurement minimizes the so-called T2 shine-through, referring to the high signal from long T2 species seen in DWI because of superimposed T2 weighting and permits evaluation of isolated diffusion effects.[4]

However, the ADC model does not distinguish between the different compartments where the water protons can move, such as intravascular, extravascular, extracellular, and intracellular spaces. If several b values are acquired less than and greater than 100 s/mm^2, it is possible to differentiate between the fast movement of intravascular water molecules with low b values (<100 s/mm^2), and the slow signal decay of diffusion signal with b values greater than 100 s/mm^2, secondary to restricted water movement in the extracellular and

intracellular compartments[8] (see Fig. 1 in the article by Broncano in this issue).[9] This model is known as Intra Voxel Incoherent Motion (IVIM) because it has been found useful in the characterization of focal liver and pancreatic lesions, with advantage over ADC measurements in some scenarios.[10,11] The contribution of true diffusion and perfusion toward signal loss is separated in this model and reflected in the following parameters: f (perfusion fraction) that represents the flowing water molecules within the capillaries; D (tissue diffusivity), a more reliable marker of tissue diffusion than ADC in organs with tissues with significant perfusion fraction; and finally, D* (pseudo-diffusion coefficient), related to the perfusion contribution to signal decay.

If ultrahigh b values greater than 1500 s/mm^2 are acquired, the remaining diffusion signal is related to a layer of polarized water molecules near of the charges of the membranes. The measurement of this very slow diffusion pool requires the use of a non-Gaussian model, such as diffusional kurtosis imaging (DKI), which reflects the microstructural complexity of tissue (see Fig. 1 in the article by Broncano in this issue). Derived parameters from DKI can help in the characterization of focal liver lesions.[12] Compared with ADC, these models provide supplementary information of the diffusion signal from other compartments different to extracellular one (Fig. 2).

b-values selection—ADC calculation minimally requires the use of 2 b values, although the more b values obtained, the better the reliability of ADC maps. In the abdomen, typically the ideal higher b value ranges between 600 and 1000 s/mm^2 in order to maintain a sufficient signal-to-noise ratio (SNR).[4] DKI requires a maximum b value in the range of 1500–2000 s/mm^2,[12] and IVIM analysis requires several b values less than and greater than 100 s/mm^2, although it is feasible even with only 3 to 4 b values.[13] However, the optimum set of b values and diffusion model used for analysis for oncological applications in the body is still to be defined.

Clinical Applications of Diffusion-Weighted Imaging

Liver

Lesion detection: DWI using a low b value around 50 s/mm^2, also known as black-blood diffusion, allows better detection of small focal liver lesions against a liver parenchyma without vessel signal[14] (Fig. 3). This type of approach has been shown to improve detection of metastases in comparison to fat-suppressed T2-weighted sequences and is of special interest for identifying metastases from colorectal cancer before surgery, with particular advantage in the detection of lesions smaller than 1 cm and those adjacent to vascular structures. Furthermore, in patients at risk for nephrogenic systemic fibrosis, DWI can be considered an alternative to contrast-enhanced imaging.[14] DWI in combination with gadoxetic acid (Gd-EOB-DTPA) improves detection of liver metastases compared with any individual technique alone, even after neoadjuvant chemotherapy.[15]

Lesion characterization: The role of DWI in focal liver lesion characterization is controversial due to misregistration between images with different b values, caused by respiratory motion. Adequate reproducibility has been achieved for ADC, but lower for f and D*.[16] DWI has been shown to accurate differentiate between cystic and solid liver lesions.

Benign lesions tend to show higher ADC values and lower SI with high b values than malignant ones (Fig. 4). However, there are no definitive data to support the use of ADC in the distinction between benign and malignant focal liver lesions, due to substantial overlap, particularly focal nodular hyperplasia (FNH) and adenomas with hepatocellular carcinoma (HCC) and metastasis. In addition, radiologists must be alert to potential pitfalls such as low ADC values seen in pyogenic abscess or high ADC values of necrotic or mucinous metastasis.[17]

IVIM-derived D and ADC show inconclusive results in the distinction of benign and malignant lesions, although with contradictory data about which of both parameters is more accurate.[10,13,18] D* and f are useful to differentiate hypervascular from hypovascular lesions.[10]

Hepatocellullar nodules in cirrhosis: DWI is of limited value in the evaluation of focal lesions in cirrhotic livers. DWI shows a lower sensitivity compared with dynamic contrast-enhanced MR imaging (DCE-MR imaging) and hepatobiliary (HB) phase in HCC detection.[19] It also does not allow differentiation between dysplastic nodules and early HCC.[20] However, DWI should be included in the protocol of detection of HCC, because it significantly improves sensitivity when used in combination with either technique.[20] Most commonly, HCC shows restriction of water diffusion, paralleling degree of cellularity and dedifferentiation. Furthermore, a recent meta-analysis concluded that DWI had excellent and moderately high diagnostic accuracy for the prediction of well-differentiated versus poorly differentiated HCC,[21] although overlap remains between different histologic grades.[22] Recently, IVIM-derived D values of HCC showed significantly better diagnostic performance than ADC values in differentiating high-grade from low-grade HCC. In addition, f demonstrated a significant correlation with the percentage of arterial enhancement of HCC.[23] Interestingly, benign lesions associated with cirrhosis, such as confluent fibrosis or perfusion alterations, do not show increased signal with high b values.[24]

Therapy monitoring: DWI has been used for early assessment of tumor response to treatment of both primary and secondary malignancies of the liver[4,5,25] (Figs. 5 and 6). The good reproducibility of ADC measurement means that any ADC changes after treatment can be related to treatment effects. In general, increases in ADC after 1 week of successful treatment can be detected in the liver.[5]

For example, DWI with ADC is useful in the early assessment of HCC response after transcatheter arterial chemoembolization (TACE), and differentiating between viable and necrotic portions of the treated HCCs.[26] Furthermore, DWI can detect recurrent tumor after treatment and predict HCC response to TACE using the monoexponential or biexponential models of analysis.[27,28]

DWI also can be used as a biomarker of treatment response of HCC to the antiangiogenic agent, sorafenib. First, ADC decreases probably related to hemorrhagic necrosis and, posteriorly, increases because of tumor necrosis. A delayed ADC decrease suggests tumor recurrence.[29] IVIM-related D and f have been shown also to be valuable markers of treatment response to sorafenib for HCC.[30]

For therapy monitoring of hepatic metastases, increases of ADC after the start of chemotherapy or radiotherapy have been related to responding metastases, although there is no defined threshold of increase in ADC to define response.[5,25] These changes can be detected during the first week after the start of treatment in colorectal and breast liver metastases and occur before changes in size.[31] In addition, DWI appears superior to positron emission tomography/computed tomography (PET/CT) for early response assessment of metastases of common solid tumors treated with Y90 radioembolization.[32] Lower pretreatment ADC value has been related to good response to chemotherapy in colorectal and gastric hepatic metastases, although these data were not confirmed in a prospective series including digestive tract and breast liver metastases.[31,33] Furthermore, low-pretreatment ADC value of colorectal liver metastases has shown an association to shorter overall survival and progression-free survival.[34]

Biliary system and gall-bladder malignancies—DWI detects intrahepatic and extrahepatic cholangiocarcinoma (CHC) with advantage over T2-weighted and in a similar manner to DCE-MR imaging. Because this lesion shows the lowest ADC of all hepatic malignancies, its differentiation from benign focal liver lesions using DWI is feasible. DWI also helps in the differentiation between mucus and viable intraductal CHC obstructing the bile duct. The lower the degree of tumor differentiation in CHC, the lower the ADC value is.[35] A target appearance on DWI, a hyperintense peripheral halo (viable tumor) with a hypointense central area (fibrosis), permits the accurate differentiation of small intrahepatic CHC from HCC, because this sign is superior to other morphologic, DCE-MR imaging, or HB phase features.[36]

As with other malignancies, gallbladder carcinoma typically demonstrates high signal on high b-value imaging, and low ADC values (Fig. 7). Acute cholecystitis may simulate a neoplastic process on DWI. For this reason, DWI must be evaluated along with the other morphologic images, increasing the accuracy in the differentiation of benign and malignant gallbladder lesions.[37]

Pancreatic cancer and other pancreatic tumors—A recent meta-analysis demonstrates high performance of DWI in detection of pancreatic adenocarcinoma (PA), with similar sensitivity to fluorodeoxyglucose (18FDG) PET/CT, but better specificity.[38] Most commonly, PA shows high SI on high b-value imaging and lower ADC values than normal pancreas, related to dense fibrosis and increased cellular elements[39] (Fig. 8). However, PA can have different appearances on diffusion imaging depending on histologic characteristics. Edematous fibrosis and loose collagen fibers have been described in PA to yield higher ADC than normal parenchyma.[40] This heterogeneity in histologic content is probably the cause of contradictory data in the relationship between ADC values of PA and tumor grade.[41,42] Moreover, the association of acute pancreatitis and PA located in the pancreatic head has been reported. Both entities show a similar behavior in DWI, hampering cancer detection.[39] The use of IVIM-derived parameters, such as f, improves the differentiation between PA and normal pancreatic tissue.[43]

DWI is also helpful in the differentiation between PA and benign lesions, although with limitations in the distinction from mass-forming pancreatitis. There is an evident overlap in

ADC values of both lesions, probably due to variable proportions of fibrosis and inflammation in mass-forming pancreatitis and different degrees of PA differentiation[39,41,42] (see Fig. 8; Fig. 9). However, initial data suggest a role for IVIM-derived perfusion parameters in this distinction.[11]

In the therapy monitoring setting, preliminary data suggest that lower pretreatment ADC values of advanced PA, treated with chemotherapy or chemoradiation, are related to poor response and early progression[44] (Fig. 10). DWI is also useful in the evaluation of autoimmune pancreatitis response to steroids. This entity shows high SI on high b value and lower ADC values than chronic pancreatitis and PA. However, with successful treatment, SI on high b value decreases, and ADC returns to normal values.[45]

Pancreatic neuroendocrine tumors (PNET) show a restrictive pattern in diffusion, in comparison with normal pancreatic parenchyma[46] (Fig. 11). However, the detection rate of PNETs with MR imaging including DWI was significantly lower than that of ^{68}Ga-DOTATATE PET/CT.[47] Most aggressive PNETs show lower ADC values than benign lesions. In addition, an inverse correlation between Ki-67 (cellular marker for proliferation) and ADC values has been established, which would allow for the evaluation of tumor aggressiveness.[46] Perfusion parameters from IVIM models are able to accurately differentiate PNET from PA.[11]

Pancreatic cystic lesions are a common incidental finding. It is important to differentiate cystic tumors from nonneoplastic lesions and identify malignant variants. Cystic tumors show different biological behavior and risk of malignancy[48] and can be classified as shown in Box 3. Cystic lesions greater than 2 cm in size are usually premalignant or malignant.[49]

DWI with high b value can differentiate nonneoplastic cysts, such as simple cysts and pseudocysts, which are usually isointense to the pancreas, from neoplastic cysts and abscesses, which remain hyperintense.[48] Boraschi and colleagues[50] found statistically significant differences in ADC values of intraductal papillary mucinous neoplasms (IPMNs), mucinous cystic neoplasms (MCNs), serous cystadenomas, and pseudocysts, although other series have shown significant overlap in the ADC values of cystic pancreatic lesions.[48] More consistent data have shown significantly higher ADC values for IPMNs compared with MCNs.[51] Furthermore, ADC and D values of malignant IPMN are significantly lower than benign variants[11] (Figs. 12 and 13). Currently, the differentiation of cystic pancreatic lesions only based on DWI remains limited, although integrated in a comprehensive MR protocol, diffusion is considered helpful.

PERFUSION MR IMAGING

A mainstay of tissue and lesion characterization in abdominal MR imaging is a DCE series, which assesses the enhancement of tissues at predetermined time points after contrast injection. The core physiology probed by this examination is perfusion, which is defined as the passage of blood through the capillary bed to deliver nutrients and oxygen to the tissue. The current clinical assessment uses 2 to 4 time points after contrast injection to visually assess enhancement patterns in organ parenchyma and lesions, which indirectly provide

valuable information about tissue physiology and pathology. One limitation to this approach is that very few images are acquired to analyze a very complex enhancement curve. The arterial phase of enhancement, in particular, can be difficult to capture because of the transient and temporally variable nature of enhancement of lesions during this phase. Moreover, this assessment is qualitative, and factors, such as the radiologist's skill, accuracy of timing after injection, and the protocol used, can inordinately affect the clinical reading. A major frontier in abdominal MR imaging is the development of an accurate quantitative DCE-MR imaging examination that enables extraction of perfusion parameters, which reflect tissue properties. Recent literature suggests that this quantitative approach has potential applications in early diagnosis of liver cirrhosis,[52,53] noninvasive diagnosis of focal lesions,[54] assessment of response to novel antiangiogenic chemotherapeutic drugs,[55–57] and in predicting treatment response in tumors as HCC[56,58,59] and PA.[60]

Technical Design of Perfusion MR Imaging of Upper Abdomen

Image acquisition—The characteristics of an ideal DCE-MR imaging perfusion examination are listed in Box 4. Gadolinium-based contrast agents (GBCAs) are used as tracers and image acquisition aims to accurately capture changes in tissue SI, which is related to changes in concentration of the GBCA over time. Both extracellular and hepatobiliary contrast agents (HBCA; Gd-EOB-DTPA) have been used for perfusion MR imaging studies.[53,61–63] Before injecting the contrast agent, a T_1 quantification acquisition is performed to determine the baseline tissue signal. This T_1 quantification acquisition is done by using the variable flip angle technique[64]; flip angles in the range of 30° to 60° are recommended.[65,66] This T_1 quantification acquisition is followed by the actual DCEMR imaging acquisition: a GBCA (0.1 mmol/kg body weight) is injected through a wide-bore cannula (20Gor larger) placed in a large antecubital vein using a power injector at a flow rate of 2 to 4 mL/s, followed by a 20 to 30 mL saline flush. Repeated T_1-weighted gradient echo imaging of the tissue of interest is performed every few seconds. The capillary transit time in well-perfused organs such as the liver is on the order of 3 to 5 seconds; hence, a sampling interval of less than 2 seconds per volume is typically required.[64,67] Multiple volumes are acquired over a period of 3 to 5 minutes, starting 10 to 20 seconds before contrast injection, to capture the change in concentration of the GBCA with time.[52,53]

Meeting the high-spatial and temporal resolution and volumetric coverage goals in a perfusion DCE-MR imaging examination requires the use of ultrafast MR imaging techniques. The fast acquisition techniques currently available in clinical practice use combinations of acceleration technologies as partial Fourier acquisitions,[68] view sharing,[69,70] and parallel imaging.[71,72] Abdominal perfusion imaging based on these technologies has been applied to characterization of focal liver lesions[54,73,74] and in assessing response in liver tumors after antiangiogenic chemotherapy.[59,75] However, dynamic imaging performed with view-sharing techniques involves direct sharing of data across frames, and thus, each image has a broad temporal footprint. Motion can thus adversely affect the images, and at least theoretically, the accuracy of perfusion modeling can also be compromised. Thus, multiple acquisition strategies are under investigation in the research setting, using non-Cartesian acquisitions, non-Cartesian parallel imaging, and compressed sensing reconstructions.[76–83]

Images may be acquired during breath-hold or using respiratory triggering so that data are acquired at the same time in the respiratory cycle. A continuous breath-hold for 3 to 5 minutes of a perfusion scan is clearly impossible—and thus multiple breath-holds may be used.[79,80] However, this results in gaps in data acquisition, which affect perfusion calculations. Imaging using respiratory cycle triggering results in lower temporal resolution, which is inadequate for calculating perfusion parameters.[81] A more practical approach is acquiring data during quiet breathing, followed by use of postprocessing image registration techniques that align the images to the same level.[78,82–85] Thus, ultrafast 3-dimensional high-resolution techniques that enable free breathing perfusion examinations have become the subject of cutting-edge work in the field.[76,77,79–82,84–87]

Data analysis—The data obtained from a perfusion study can be analyzed in 3 ways: visual assessment, semiquantitative assessment, or a quantitative analysis.[65] These approaches are briefly described in Table 2, along with pros and cons of each approach. Visual assessment is a qualitative evaluation of enhancement pattern of the lesion by the radiologist. The semiquantitative methods track change in tissue SI over time to provide parameters as time to peak enhancement, maximum enhancement, wash-in slope, washout slope, arterial perfusion index (defined as proportion of perfusion derived from an artery, for example, hepatic perfusion index for hepatic artery),[74] mean transit time (MTT), and area under the curve (AUC).[88,89] Quantitative methods allow conversion of SI-time curves to concentration-time curves, which are then modeled using knowledge of tracer pharmacokinetics to derive tissue properties as perfusion and permeability.[90] The perfusion parameters are finally calculated by voxel or region-of-interest (ROI) analysis.

Although multiple methods to model data have been described, most commonly used are compartment models,[65] which are discussed in this review. There is some variability in the literature regarding usage of the term compartment. Some authors consider vessels supplying the tissue as one compartment and the extravascular, extracellular space (EES) in the tissue as a second compartment.[74,91] Others define vessels as an input and restrict the term compartment to the EES, where actual exchange of plasma occurs.[75,92] In this discussion, the latter convention is followed. The GBCAs diffuse freely across the blood vessel wall into the EES. The movement of GBCAs from circulation into the EES and then back into the venous system for clearance describes the physiologic properties of a tissue or vascular properties of a lesion. This movement is described in terms of compartment volumes and rate of transfer of GBCAs between the compartments. As most tracers are not taken up by cells, v_e represents volume of EES per unit volume of tissue. The transfer constant of GBCA from plasma into EES is called K^{trans} (forward volume transfer constant), and it depends on tissue permeability and flow. In high-permeability tissues such as liver, it measures the flow of contrast from the microvasculature into the EES; in high-flow conditions, it represents the permeability.[93] Finally, the rate constant k_{ep} represents the return of contrast from the EES to the vessels and is obtained as a ratio of K^{trans} and v_e. In most tissues, there is a single artery supplying the tissues—a single-input, single-compartment model is applied. The compartment model can be adapted according to variations in the arterial supply in organs and number of tissue compartments perfused: a dual-input, single-compartment model is often used in the liver where dual input is derived

from hepatic artery and portal vein and the tissue perfused is liver parenchyma; a single-input, dual-compartment model is applied in the kidney where input is derived from renal artery, and glomeruli and tubules form the 2 tissue compartments. Based on the tissue evaluated and the model used, parameters such as arterial fraction, venous fraction, total blood flow, distribution volume (DV), MTT, and capillary permeability-surface area product (PS) can be derived (Fig. 14).

Although quantitative DCE-MR imaging methods have some advantages over visual assessment or semiquantitative methods, variations in physiologic assumptions made at the outset and the choice of mathematical models can influence the values of derived quantitative parameters. Another major limitation is that there are no universally accepted acquisition methods, mathematical models, and software for calculation of perfusion parameters. Hence, these methods suffer from poor reproducibility, and it is difficult to compare results from different studies. Moreover, image acquisition, reconstruction, registration, and postprocessing techniques for most of the methods described thus far are complicated and time- and labor-intensive. Current efforts are geared toward development of standardized image acquisition and data analysis models so that these powerful techniques can gain wider acceptance in abdominal imaging.

Clinical Applications of Dynamic Contrast-Enhanced-MR Imaging

Liver—Both semiquantitative and quantitative methods have been applied for assessment of perfusion in liver in various disease states.[73] It has been shown that the hepatic perfusion index, that is, the fraction of perfusion derived from the hepatic artery, is different in patients with and without metastases[84,94] (see Fig. 14), even when the metastases are not macroscopically visible.[95] Also, metastases were found to have a finite PS and interstitial space volume, in contrast to normal liver, which has near zero PS and interstitial space volume.[63] Perfusion MR imaging in patients receiving bevacizumab-based chemotherapy for colorectal cancer metastases to liver revealed that a decrease in K^{trans} and k_{ep} ratios correlated with treatment response as early as 1 week after therapy.[96]

HCC is characterized by neoangiogenesis and derives most of its blood supply from the hepatic artery; this is reflected in the MR perfusion studies as increased hepatic arterial flow, total blood flow, and PS compared with metastases.[54,91] DCE-MR imaging has been used as an imaging biomarker to assess the effectiveness of various treatment modalities. These changes have been documented with standard cytotoxic therapies,[58,59] radiotherapy,[97] as well as with use of antiangiogenic drugs as bevacizumab[56] and antivascular endothelial growth factor tyrosine kinase inhibitor sorafenib.[55,57] Various authors have reported significant changes in perfusion parameters that correlate with treatment response as well as disease outcome.[55–59,97] A decrease in K^{trans} was the most useful measure that predicted prolonged survival.[55,58] It has been suggested that a 40% decrease in K^{trans} correlates with significant drug effect.[98]

Pancreas—Perfusion MR imaging of the pancreas has been performed using radial k-space sampling gradient-echo sequence with k-space-weighted image contrast.[99,100] A significant difference ($P<.0001$) was found in K^{trans}, k_{ep}, and AUC values for pancreatic

cancer, neuroendocrine tumors, chronic pancreatitis, and normal pancreas[100] (Fig. 15). In addition, it was found that K^{trans} values for pancreatic cancer, and for apparently normal pancreatic parenchyma adjacent to the tumor, was significantly lower in patients who developed a recurrence than those who did not. This finding reflects the fact that pancreatic cancer is a hypovascular tumor and K^{trans} values reflect blood flow. Thus, perfusion MR imaging has a potential role in the characterization of solid pancreatic masses, which frequently have overlapping imaging features.

Perfusion MR imaging has also been studied in evaluating response after antiangiogenic chemotherapy in locally advanced pancreatic cancer; pretreatment K^{trans} and k_{ep} values were found to be significantly higher in tumors that showed marked response compared with those that did not respond.[60]

Cholangiocarcinoma—The utility of perfusion MR imaging in assessing response to intra-arterial chemotherapy in patients with unresectable, intrahepatic CHC has been evaluated in a single clinical trial.[101] It was found that patients with a higher AUC at 90 and 180 seconds had a longer disease-free survival (Fig. 16). Hence, AUC can be an imaging biomarker that helps select patients who would benefit the most from intra-arterial chemotherapy.

ARTERIAL SPIN LABELING

Arterial spin labeling (ASL) has proven useful to quantify blood flow in brain, prostate, and renal tumors.[102,103] This noncontrast technique allows quantifying blood flow using arterial water as an endogenous contrast agent. A flow-sensitized image (labeled image) is subtracted from a control image in order to obtain a difference (subtraction) image, which reflects the tissue (and lesion) perfusion, as all the signal from the stationary tissue is the same in both images, and therefore, completely suppressed during the subtraction process. Water protons of the blood supplying the liver are saturated using a radiofrequency inversion pulse; when these labeled spins reach the capillaries of the liver, they are exchanged with tissue water, originating the perfusion signal.

There are different technical approaches such as low-sensitive alternating inversion recovery (FAIR) and pseudocontinuous ASL acquisitions that permit the detection of flow and its quantification. Limited experience is accumulated in the upper abdomen because this technique is complex and very sensitive to breathing artifacts.[104–106] Recent data suggest a role for this technique in the differentiation between solid and cystic liver lesions.[107] Furthermore, ASL has been proven useful for therapy monitoring of renal cell carcinoma treated with antiangiogenic drugs, opening a window for their use for other malignancies of the upper abdomen[104] (Fig. 17).

^{1}H-MAGNETIC RESONANCE SPECTROSCOPY

MR spectroscopy (MRS) can explore in vivo the pathophysiology and metabolism of tumors. This technique analyzes the tissue chemical composition of different molecules present in the voxel using nuclei such as phosphorus (^{31}P), carbon (^{13}C), and hydrogen (^{1}H).

This last nucleus is the only nucleus that is readily analyzed in clinical practice, because it shows the highest sensitivity and SNR and does not require special hardware or equipment.[108] Box 5 summarizes the main technical characteristics of in vivo ^{1}H-MRS for liver tumor assessment, which is very challenging.

The detection of a choline peak at 3.2 ppm, a biomarker of tumor proliferation, is consistent with malignancy[109] (Fig. 18). In general, the greater the choline peak, the less differentiated the tumor. In vitro ^{1}H-MRS has shown excellent results in the differentiation of HCC from cirrhotic liver,[110] but these results have not been confirmed for in vivo ^{1}H-MRS of liver tumors. Increased choline resonances were found in malignant liver tumors compared with uninvolved liver or benign lesions, but without statistical difference in mean choline/lipid ratio.[109] Conversely, the data from Fischbach and colleagues[111] showed reduced choline signal relative to that of water in metastatic lesions, without significant differences between malignant liver tumors and normal liver. These contradictory data can be due to multiple contributions to the total choline signal from choline, phosphocholine, glycerophosphocholine, and taurine, which are different in normal liver and malignant tumors, but not detectable with ^{1}H-MRS.[108] However, preliminary data suggest a possible role for ^{1}H-MRS in therapy monitoring of HCC, as an early drop in choline peak is identified in responding HCC to TACE.[109] The use of multivoxel acquisition, fat suppression, and 7-T magnets will probably improve these initial results.[112]

MAGNETIC RESONANCE ELASTOGRAPHY

MR elastography (MRE) has been applied mostly in the detection and grading of liver fibrosis because this technique allows the assessment of liver parenchyma stiffness. MRE requires specialized hardware and software, which has limited its clinical use. Low-frequency (50–60 Hz) mechanical shear waves are generated via an active audio driver outside the MR suite, which are transmitted to a passive driver placed over the liver. A modified phase-contrast sequence is used to image the propagating waves (wave image), which is then processed with an inversion algorithm to generate a quantitative image of shear stiffness (elastogram) measured in kilopascals. These shear waves propagate more rapidly in stiffer tissue and more slowly in softer tissue, and as they are applied continuously, the wavelength is longer in stiffer tissues.[6]

MRE has also been tested for characterization of liver tumors, because malignant tumors show significantly higher mean shear stiffness than benign ones (Fig. 19). Preliminary data suggest that cutoff values of 5 kPa accurately differentiated malignant tumors from benign tumors and normal liver parenchyma.[6] These results are similar to those obtained using acoustic radiation-forced imaging elastography. In addition, MRE can also differentiate the viscoelastic components of liver tumors by analyzing the complex-valued shear modules separately. Increased viscosity has been reported in malignant liver tumors. Moreover, a potential role for MRE in the early assessment of tumor response to vascular disrupting agents and chemotherapy in animal models has been proposed.[113] Larger studies are necessary to confirm these promising preliminary results.

HEPATOBILIARY CONTRAST AGENTS

HBCAs have both extracellular behavior and a hepatocyte-specific delayed phase, which improves detection and characterization of focal liver lesions.[25] There are 2 commercially available agents in the United States (Table 3). Gd-EOB-DTPA shows greater hepatocellular uptake and biliary excretion than gadobenate dimeglumine (Gd-BOPTA), which has resulted in more extended use and more reported clinical experience in recent years. Table 4 summarizes some key characteristics of both contrast agents.

Boxes 6 and 7 summarize the normal appearance of common solid benign and malignant focal liver lesions (except hemangioma) and the current clinical applications in oncology of HBCA, respectively. Currently, HBCA have a defined role in the preoperative assessment of colorectal cancer liver metastasis, as they increase its detection compared with other imaging techniques, improving even more their results if they are used in combination with DWI[7,15,114] (Fig. 20). HB images do not rely on lesion vascularity, which is a significant advantage in the posttherapeutic setting, as after neoadjuvant chemotherapy the detection rates of metastases with MR imaging are lowered, although they are still superior to other imaging methods.[15] Hence, the use of Gd-EOB-DTPA provides accurate preoperative staging and detection rates similar to pretreatment imaging.[15]

Both HBCA perform similarly in the detection of HCC,[115] with initial data supporting improvements compared with dynamic MR imaging with GBCAs for the detection of small HCC (<2 cm)[15,116] (Fig. 21). Furthermore, HBCAs help in the staging and histologic grading of this tumor, although there is still a need for larger multicenter trials to define their usefulness in this task.[7,15] Better defined is the role of these contrast agents in the differentiation between adenoma and FNH, as their use improves the differentiation of these 2 entities compared with GBCAs[117,118] (Figs. 22 and 23). HBCAs are also of interest in the postoperative assessment of biliary or traumatic leaks.[7] More recently, decreased excretion of Gd-EOBDTPA has been demonstrated in the setting of impaired HB function, which can be quantified. In this manner, this contrast agent has the potential to assess the risk for liver failure after major liver resection.[113]

MULTIPARAMETRIC IMAGING

MR imaging explores different functional and molecular information of HBP malignancies in a single examination. Therefore, the combination of these different quantitative parameters can help gain insight into tumor biology. Measurement of changes in tumor characteristics with treatment can help in therapy monitoring, radiotherapy planning, and drug development. Furthermore, the combined use of MR imaging-derived parameters with other functional techniques such as CT perfusion or PET can improve results and will be enhanced with the use of new hybrid technology such as PET-MR imaging. MPI is in its infancy, and further research is needed to enhance its role in the management of abdominal malignancies.

SUMMARY

MR imaging provides multiple imaging biomarkers for the assessment of HBP malignancies, which can be integrated in a comprehensive protocol tailored to the clinical problem. These techniques are at various stages of clinical adoption, as many are technically demanding and lack sufficient standardization and still require further validation. The potential of all these techniques is enhanced if an MPI approach is used to assess tumor behavior.

Acknowledgments

Dr V. Gulani has an NIH Grant: 1R01DK098503, and receives research support from Siemens Healthcare. Drs S. Pahwa and K.L. Wright receive research support from Siemens Healthcare. Dr A. Luna and Dr Bonini C has nothing to disclose.

REFERENCES

1. Bartolozzi C, Lencioni R, Donati F, et al. liver and pancreas. Eur Radiol. 1999; 9(8):1496–1551. [PubMed: 10525857]
2. Eisenhauer EA, Therasse P, Bogaerts J, et al. New response evaluation criteria in solid tumours: revised RECIST guideline (version 1.1). Eur J Cancer. 2009; 45(2):228–247. [PubMed: 19097774]
3. Wahl RL, Jacene H, Kasamon Y, et al. From RECIST to PERCIST: evolving considerations for PET response criteria in solid tumors. J Nucl Med. 2009; 50(Suppl 1):122–150.
4. Padhani AR, Liu G, Koh DM, et al. Diffusion-weighted magnetic resonance imaging as a cancer biomarker: consensus and recommendations. Neoplasia. 2009; 11(2):102–125. [PubMed: 19186405]
5. Goh V, Gourtsoyianni S, Koh DM. Functional imaging of the liver. Semin Ultrasound CT MR. 2013; 34(1):54–65. [PubMed: 23395318]
6. Venkatesh SK, Yin M, Glockner JF, et al. MR elastography of liver tumors: preliminary results. AJR Am J Roentgenol. 2008; 190(6):1534–1540. [PubMed: 18492904]
7. Lebedis C, Luna A, Soto JA. Use of magnetic resonance imaging contrast agents in the liver and biliary tract. Magn Reson Imaging Clin N Am. 2012; 20(4):715–737. [PubMed: 23088947]
8. Luciani A, Vignaud A, Cavet M, et al. Liver cirrhosis: intravoxel incoherent motion MR imaging—pilot study. Radiology. 2008; 249(3):891–899. [PubMed: 19011186]
9. Broncano J, Alcalá AL, González J, et al. Functional MR Imaging in Chest Malignancies. Magn Reson Imaging Clin N Am. 2016 in press.
10. Yoon JH, Lee JM, Yu MH, et al. Evaluation of hepatic focal lesions using diffusion-weighted MR imaging: comparison of apparent diffusion coefficient and intravoxel incoherent motion-derived parameters. J Magn Reson Imaging. 2014; 39(2):276–285. [PubMed: 23633178]
11. Kang KM, Lee JM, Yoon JH, et al. Intravoxel incoherent motion diffusion-weighted MR imaging for characterization of focal pancreatic lesions. Radiology. 2014; 270(2):444–453. [PubMed: 24126370]
12. Rosenkzrantz AB, Padhani AR, Chevenert TL, et al. Body diffusion kurtosis imaging: Basic principles, applications, and considerations for clinical practice. J Magn Reson Imaging. 2015
13. Penner AH, Sprinkart AM, Kukuk GM, et al. Intravoxel incoherent motion model-based liver lesion characterisation from three b-value diffusion-weighted MRI. Eur Radiol. 2013; 23(10): 2773–2783. [PubMed: 23666233]
14. Hardie AD, Naik M, Hecht EM, et al. Diagnosis of liver metastases: value of diffusion-weighted MRI compared with gadolinium-enhanced MRI. Eur Radiol. 2010; 20(6):1431–1441. [PubMed: 20148251]
15. Jhaveri K, Cleary S, Audet P, et al. Consensus statements from a multidisciplinary expert panel on the utilization and application of a liver-specific MRI contrast agent (gadoxetic acid). AJR Am J Roentgenol. 2015; 204(3):498–509. [PubMed: 25714278]

16. Kakite S, Dyvorne H, Besa C, et al. Hepatocellular carcinoma: short-term reproducibility of apparent diffusion coefficient and intravoxel incoherent motion parameters at 3.0T. J Magn Reson Imaging. 2015; 41(1):149–156. [PubMed: 24415565]
17. Bittencourt LK, Matos C, Coutinho AC Jr. Diffusion-weighted magnetic resonance imaging in the upper abdomen: technical issues and clinical applications. Magn Reson Imaging Clin N Am. 2011; 19(1):111–131. [PubMed: 21129638]
18. Doblas S, Wagner M, Leitao HS, et al. Characterizing focal hepatic lesions by free-breathing intravoxel incoherent motion MRI at 3.0 T. Invest Radiol. 2013; 48(10):722–728. [PubMed: 23669588]
19. Faletti R, Cassinis MC, Fonio P, et al. Multiparametric Gd-EOB-DTPA magnetic resonance in diagnosis of HCC: dynamic study, hepatobiliary phase, and diffusion-weighted imaging compared to histology after orthotopic liver transplantation. Abdom Imaging. 2015; 40(1):46–55. [PubMed: 24965896]
20. Hwang J, Kim YK, Kim JM, et al. Pretransplant diagnosis of hepatocellular carcinoma by gadoxetic acid-enhanced and diffusion-weighted magnetic resonance imaging. Liver Transpl. 2014; 20(12):1436–1446. [PubMed: 25103727]
21. Chen J, Wu M, Liu R, et al. Preoperative evaluation of the histological grade of hepatocellular carcinoma with diffusion-weighted imaging: a meta-analysis. PLoS One. 2015; 10(2):e0117661. [PubMed: 25658359]
22. Nishie A, Tajima T, Asayama Y, et al. Diagnostic performance of apparent diffusion coefficient for predicting histological grade of hepatocellular carcinoma. Eur J Radiol. 2011; 80(2):29–33.
23. Woo S, Lee JM, Yoon JH, et al. Intravoxel incoherent motion diffusion-weighted MR imaging of hepatocellular carcinoma: correlation with enhancement degree and histologic grade. Radiology. 2014; 270(3):758–767. [PubMed: 24475811]
24. Motosugi U, Ichikawa T, Sou H, et al. Distinguishing hypervascular pseudolesions of the liver from hypervascular hepatocellular carcinomas with gadoxetic acid-enhanced MR imaging. Radiology. 2010; 256(1):151–158. [PubMed: 20574092]
25. deSouza DA, Parente DB, de Araújo AL, et al. Modern imaging evaluation of the liver: emerging MR imaging techniques and indications. Magn Reson Imaging Clin N Am. 2013; 21(2):337–363. [PubMed: 23642557]
26. Chung JC, Naik NK, Lewandowski RJ, et al. Diffusion-weighted magnetic resonance imaging to predict response of hepatocellular carcinoma to chemoembolization. World J Gastroenterol. 2010; 16(25):3161–3167. [PubMed: 20593501]
27. Mannelli L, Kim S, Hadju CH, et al. Serial diffusion-weighted MRI in patients with hepatocellular carcinoma: prediction and assessment of response to transarterial chemoembolization. Preliminary experience. Eur J Radiol. 2013; 82(4):577–582. [PubMed: 23246330]
28. Park YS, Lee CH, Kim JH, et al. Using intravoxel incoherent motion (IVIM) MR imaging to predict lipiodol uptake in patients with hepatocellular carcinoma following transcatheter arterial chemoembolization: a preliminary result. Magn Reson Imaging. 2014; 32(6):638–646. [PubMed: 24703575]
29. Schraml C, Schwenzer NF, Martirosian P, et al. Diffusion-weighted MRI of advanced hepatocellular carcinoma during sorafenib treatment: initial results. AJR Am J Roentgenol. 2009; 193(4):W301–W307. [PubMed: 19770299]
30. Lewin M, Fartoux L, Vignaud A, et al. The diffusion-weighted imaging perfusion fraction f is a potential marker of sorafenib treatment in advanced hepatocellular carcinoma: a pilot study. Eur Radiol. 2011; 21(2):281–290. [PubMed: 20683597]
31. Koh DM, Scurr E, Collins D, et al. Predicting response of colorectal hepatic metastasis: value of pretreatment apparent diffusion coefficients. AJR Am J Roentgenol. 2007; 188(4):1001–1008. [PubMed: 17377036]
32. Barabasch A, Kraemer NA, Ciritsis A, et al. Diagnostic accuracy of diffusion-weighted magnetic resonance imaging versus positron emission tomography/computed tomography for early response assessment of liver metastases to y90-radioembolization. Invest Radiol. 2015; 50(6):409–415. [PubMed: 25763526]

33. Mungai F, Pasquinelli F, Mazzoni LN, et al. Diffusion-weighted magnetic resonance imaging in the prediction and assessment of chemotherapy outcome in liver metastases. Radiol Med. 2014; 119(8):625–633. [PubMed: 24408046]
34. Heijmen L, ter Voert EE, Oyen WJ, et al. Multimodality imaging to predict response to systemic treatment in patients with advanced colorectal cancer. PLoS One. 2015; 10(4):e0120823. [PubMed: 25831053]
35. Cui XY, Chen HW, Cai S, et al. Diffusion-weighted MR imaging for detection of extrahepatic cholangiocarcinoma. Eur J Radiol. 2012; 81(11):2961–2965. [PubMed: 22285604]
36. Park HJ, Kim YK, Park MJ, et al. Small intrahepatic mass-forming cholangiocarcinoma: target sign on diffusion weighted imaging for differentiation from hepatocellular carcinoma. Abdom Imaging. 2013; 38(4):793–801. [PubMed: 22829097]
37. Kim SJ, Lee JM, Kim H, et al. Role of diffusion-weighted magnetic resonance imaging in the diagnosis of gallbladder cancer. J Magn Reson Imaging. 2013; 38(1):127–137. [PubMed: 23281048]
38. Wu LM, Hu JN, Hua J, et al. Diagnostic value of diffusion-weighted magnetic resonance imaging compared with fluorodeoxyglucose positron emission tomography/computed tomography for pancreatic malignancy: a meta-analysis using a hierarchical regression model. J Gastroenterol Hepatol. 2012; 27(6):1027–1035. [PubMed: 22414092]
39. Muraoka N, Uematsu H, Kimura H, et al. Apparent diffusion coefficient in pancreatic cancer: characterization and histopathological correlations. J Magn Reson Imaging. 2008; 27(6):1302–1308. [PubMed: 18504750]
40. Fukukura Y, Takumi K, Kamimura K, et al. Pancreatic adenocarcinoma: variability of diffusion-weighted MR imaging findings. Radiology. 2012; 263(3):732–740. [PubMed: 22623694]
41. Rosenkrantz AB, Matza BW, Sabach A, et al. Pancreatic cancer: lack of association between apparent diffusion coefficient values and adverse pathological features. Clin Radiol. 2013; 68(4):e191–e197. [PubMed: 23312674]
42. Wang Y, Chen ZE, Nikolaidis P, et al. Diffusion-weighted magnetic resonance imaging of pancreatic adenocarcinomas: association with histopathology and tumor grade. J Magn Reson Imaging. 2011; 33(1):136–142. [PubMed: 21182131]
43. Lemke A, Laun FB, Klauss M, et al. Differentiation of pancreas carcinoma from healthy pancreatic tissue using multiple b-values: comparison of apparent diffusion coefficient and intravoxel incoherent motion derived parameters. Invest Radiol. 2009; 44(12):769–777. [PubMed: 19838121]
44. Cuneo KC, Chenevert TL, Ben-Josef E, et al. A pilot study of diffusion-weighted MRI in patients undergoing neoadjuvant chemoradiation for pancreatic cancer. Transl Oncol. 2014; 7(5):644–649. [PubMed: 25389460]
45. Muhi A, Ichikawa T, Motosugi U, et al. Mass-forming autoimmune pancreatitis and pancreatic carcinoma: differential diagnosis on the basis of computed tomography and magnetic resonance cholangiopancreatography, and diffusion-weighted imaging findings. J Magn Reson Imaging. 2012; 35(4):827–836. [PubMed: 22069025]
46. Wang Y, Chen ZE, Yaghmai V, et al. Diffusion-weighted MR imaging in pancreatic endocrine tumors correlated with histopathologic characteristics. J Magn Reson Imaging. 2011; 33(5):1071–1079. [PubMed: 21509863]
47. Schmid-Tannwald C, Schmid-Tannwald CM, Morelli JN, et al. Comparison of abdominal MRI with diffusion-weighted imaging to ^{68}Ga-DOTATATE PET/CT in detection of neuroendocrine tumors of the pancreas. Eur J Nucl Med Mol Imaging. 2013; 40(6):897–907. [PubMed: 23460395]
48. Wang Y, Miller FH, Chen ZE, et al. Diffusion-weighted MR imaging of solid and cystic lesions of the pancreas. Radiographics. 2011; 31(3):47–64.
49. Karatzas T, Dimitroulis D, Charalampoudos P, et al. Management of cystic and solid pancreatic incidentalomas: a review analysis. J BUON. 2013; 18(1):17–24. [PubMed: 23613384]
50. Boraschi P, Donati F, Gigoni R, et al. Diffusion-weighted MRI in the characterization of cystic pancreatic lesions: usefulness of ADC values. Magn Reson Imaging. 2010; 28(10):1447–1455. [PubMed: 20864287]

51. Fatima Z, Ichikawa T, Motosugi U, et al. Magnetic resonance diffusion-weighted imaging in the characterization of pancreatic mucinous cystic lesions. Clin Radiol. 2011; 66(2):108–111. [PubMed: 21216325]
52. Chen B-B, Hsu C-Y, Yu C-W, et al. Dynamic contrast-enhanced magnetic resonance imaging with Gd-EOB-DTPA for the evaluation of liver fibrosis in chronic hepatitis patients. Eur Radiol. 2012; 22(1):171–180. [PubMed: 21879400]
53. Annet L, Materne R, Danse E, et al. Hepatic flow parameters measured with MR imaging and Doppler US: correlations with degree of cirrhosis and portal hypertension. Radiology. 2003; 229(2):409–414. [PubMed: 12970464]
54. Abdullah SS, Pialat JB, Wiart M, et al. Characterization of hepatocellular carcinoma and colorectal liver metastasis by means of perfusion MRI. J Magn Reson Imaging. 2008; 28(2):390–395. [PubMed: 18666145]
55. Hsu C-Y, Shen Y-C, Yu C-W, et al. Dynamic contrast-enhanced magnetic resonance imaging biomarkers predict survival and response in hepatocellular carcinoma patients treated with sorafenib and metronomic tegafur/uracil. J Hepatol. 2011; 55(4):858–865. [PubMed: 21338641]
56. Yopp AC, Schwartz LH, Kemeny N, et al. Antiangiogenic therapy for primary liver cancer: correlation of changes in dynamic contrast-enhanced magnetic resonance imaging with tissue hypoxia markers and clinical response. Ann Surg Oncol. 2011; 18(8):2192–2199. [PubMed: 21286939]
57. Zhu AX, Sahani DV, Duda DG, et al. Efficacy, safety, and potential biomarkers of sunitinib monotherapy in advanced hepatocellular carcinoma: a phase II study. J Clin Oncol. 2009; 27:3027–3035. [PubMed: 19470923]
58. Jarnagin WR, Schwartz LH, Gultekin DH, et al. Regional chemotherapy for unresectable primary liver cancer: results of a phase II clinical trial and assessment of DCE-MRI as a biomarker of survival. Ann Oncol. 2009; 20(9):1589–1595. [PubMed: 19491285]
59. Wang J, Chen LT, Tsang YM, et al. Dynamic contrast-enhanced MRI analysis of perfusion changes in advanced hepatocellular carcinoma treated with an antiangiogenic agent: a preliminary study. AJR Am J Roentgenol. 2004; 183:713–719. [PubMed: 15333360]
60. Akisik MF, Sandrasegaran K, Bu G, et al. Pancreatic cancer: utility of dynamic contrast-enhanced MR imaging in assessment of antiangiogenic therapy. Radiology. 2010; 256(2):441–449. [PubMed: 20515976]
61. Scharf J, Zapletal C, Hess T, et al. Assessment of hepatic perfusion in pigs by pharmacokinetic analysis of dynamic MR images. J Magn Reson Imaging. 1999; 9:568–572. [PubMed: 10232516]
62. Sourbron S, Sommer WH, Reiser MF, et al. Combined quantification of liver perfusion and function with dynamic gadoxetic acid-enhanced MR imaging. Radiology. 2012; 263:874–883. [PubMed: 22623698]
63. Koh TS, Thng CH, Lee PS, et al. Hepatic metastases: in vivo assessment of perfusion parameters at dynamic contrast-enhanced MR imaging with dual-input two-compartment tracer kinetics model. Radiology. 2008; 249:307–320. [PubMed: 18695207]
64. Wang HZ, Riederer SJ, Lee JN. Optimizing the precision in T1 relaxation estimation using limited flip angles. Magn Reson Med. 1987; 5:399–416. [PubMed: 3431401]
65. Sourbron S. Technical aspects of MR perfusion. Eur J Radiol. 2010; 76:304–313. [PubMed: 20363574]
66. Judd RM, Reeder SB, Atalar E, et al. Amagnetization-driven gradient echo pulse sequence for the study of myocardial perfusion. Magn Reson Med. 1995; 34:276–282. [PubMed: 7476088]
67. Goh V, Liaw J, Bartram CI, et al. Effect of temporal interval between scan acquisitions on quantitative vascular parameters in colorectal cancer: implications for helical volumetric perfusion CT techniques. AJR Am J Roentgenol. 2008; 191(6):W288–W292. [PubMed: 19020217]
68. Margosian P, Schmitt F. Faster MR imaging: imaging with half the data. Heal Care Instrum. 1986; 1:195–197.
69. Jones RA, Haraldseth O, Müller TB, et al. K-space substitution: a novel dynamic imaging technique. Magn Reson Med. 1993; 29:830–834. [PubMed: 8350729]

70. Song T, Laine AF, Chen Q, et al. Optimal k-space sampling for dynamic contrast-enhanced MRI with an application to MR renography. Magn Reson Med. 2009; 61:1242–1248. [PubMed: 19230014]
71. Griswold MA, Jakob PM, Heidemann RM, et al. Generalized autocalibrating partially parallel acquisitions (GRAPPA). Magn Reson Med. 2002; 47:1202–1210. [PubMed: 12111967]
72. Pruessmann KP, Weiger M, Scheidegger MB, et al. SENSE: sensitivity encoding for fast MRI. Magn Reson Med. 1999; 42:952–962. [PubMed: 10542355]
73. Rao S-X, Chen C-Z, Liu H, et al. Three-dimensional whole-liver perfusion magnetic resonance imaging in patients with hepatocellular carcinomas and colorectal hepatic metastases. BMC Gastroenterol. 2013; 13:53. [PubMed: 23530688]
74. Thng CH, Koh TS, Collins DJ, et al. Perfusion magnetic resonance imaging of the liver. World J Gastroenterol. 2010; 16:1598–1609. [PubMed: 20355238]
75. Chandarana H, Taouli B. Diffusion and perfusion imaging of the liver. Eur J Radiol. 2010; 76:348–358. [PubMed: 20399054]
76. Bultman EM, Brodsky EK, Horng DE, et al. Quantitative hepatic perfusion modeling using DCE-MRI with sequential breathholds. J Magn Reson Imaging. 2014; 39:853–865. [PubMed: 24395144]
77. Salmani Rahimi M, Korosec FR, Wang K, et al. Combined dynamic contrast-enhanced liver MRI and MRA using interleaved variable density sampling. Magn Reson Med. 2015; 73(3):973–983. [PubMed: 24639130]
78. Feng L, Grimm R, Block KT, et al. Golden-angle radial sparse parallel MRI: combination of compressed sensing, parallel imaging, and golden-angle radial sampling for fast and flexible dynamic volumetric MRI. Magn Reson Med. 2014; 72(3):707–717. [PubMed: 24142845]
79. Hagiwara M, Rusinek H, Lee VS, et al. Advanced liver fibrosis: diagnosis with 3D whole-liver perfusion MR imaging–initial experience. Radiology. 2008; 246:926–934. [PubMed: 18195377]
80. Miyazaki K, Orton MR, Davidson RL, et al. Neuroendocrine tumor liver metastases: use of dynamic contrast-enhanced MR imaging to monitor and predict radiolabeled octreotide therapy response. Radiology. 2012; 263:139–148. [PubMed: 22344403]
81. Michaely HJ, Sourbron SP, Buettner C, et al. Temporal constraints in renal perfusion imaging with a 2-compartment model. Invest Radiol. 2008; 43:120–128. [PubMed: 18197064]
82. Materne R, Smith AM, Peeters F, et al. Assessment of hepatic perfusion parameters with dynamic MRI. Magn Reson Med. 2002; 47:135–142. [PubMed: 11754452]
83. Chandarana H, Feng L, Block TK, et al. Free-breathing contrast-enhanced multiphase MRI of the liver using a combination of compressed sensing, parallel imaging, and golden-angle radial sampling. Invest Radiol. 2013; 48(1):10–16. [PubMed: 23192165]
84. Mendichovszky IA, Cutajar M, Gordon I. Reproducibility of the aortic input function (AIF) derived from dynamic contrast-enhanced magnetic resonance imaging (DCE-MRI) of the kidneys in a volunteer study. Eur J Radiol. 2009; 71(3):576–581. [PubMed: 19004588]
85. Chen Y, Lee GR, Wright KL, et al. Free-breathing liver perfusion imaging using 3-dimensional through-time spiral generalized autocalibrating partially parallel acquisition acceleration. Invest Radiol. 2015; 50(6):367–375. [PubMed: 25946703]
86. Michoux N, Montet X, Pechère A, et al. Parametric and quantitative analysis of MR renographic curves for assessing the functional behaviour of the kidney. Eur J Radiol. 2005; 54(1):124–135. [PubMed: 15797302]
87. Brodsky EK, Bultman EM, Johnson KM, et al. High-spatial and high-temporal resolution dynamic contrast-enhanced perfusion imaging of the liver with time-resolved three-dimensional radial MRI. Magn Reson Med. 2014; 71(3):934–941. [PubMed: 23519837]
88. Ho VB, Allen SF, Hood MN, et al. Renal masses: quantitative assessment of enhancement with dynamic MR imaging. Radiology. 2002; 224(3):695–700. [PubMed: 12202701]
89. Scharf J, Kemmling A, Hess T, et al. Assessment of hepatic perfusion in transplanted livers by pharmacokinetic analysis of dynamic magnetic resonance measurements. Invest Radiol. 2007; 42(4):224–229. [PubMed: 17351428]
90. Brix G, Lucht R, Griebel J. Tracer kinetic analysis of signal time series from dynamic contrast-enhanced MR imaging. Biomed Tech (Berl). 2006; 51(5–6):325–330. [PubMed: 17155868]

91. Chen B-B, Shih TT-F. DCE-MRI in hepatocellular carcinoma-clinical and therapeutic image biomarker. World J Gastroenterol. 2014; 20(12):3125–3134. [PubMed: 24695624]
92. Sourbron SP, Buckley DL. Tracer kinetic modelling in MRI: estimating perfusion and capillary permeability. Phys Med Biol. 2011; 57(2):R1–R33. [PubMed: 22173205]
93. Tofts PS, Brix G, Buckley DL, et al. Estimating kinetic parameters from dynamic contrast-enhanced T1-weighted MRI of a diffusable tracer: standardized quantities and symbols. J Magn Reson Imaging. 1999; 10(3):223–232. [PubMed: 10508281]
94. Totman JJ, O'Gorman RL, Kane PA, et al. Comparison of the hepatic perfusion index measured with gadolinium-enhanced volumetric MRI in controls and in patients with colorectal cancer. Br J Radiol. 2005; 78(926):105–109. [PubMed: 15681320]
95. Tsushima Y, Blomley MJK, Yokoyama H, et al. Does the presence of distant and local malignancy alter parenchymal perfusion in apparently disease-free areas of the liver? Dig Dis Sci. 2001; 46(10):2113–2119. [PubMed: 11680584]
96. Hirashima Y, Yamada Y, Tateishi U, et al. Pharmacokinetic parameters from 3-Tesla DCE-MRI as surrogate biomarkers of antitumor effects of bevacizumab plus FOLFIRI in colorectal cancer with liver metastasis. Int J Cancer. 2012; 130(10):2359–2365. [PubMed: 21780098]
97. Liang P-C, Ch'ang H-J, Hsu C, et al. Dynamic MRI signals in the second week of radiotherapy relate to treatment outcomes of hepatocellular carcinoma: a preliminary result. Liver Int. 2007; 27(4):516–528. [PubMed: 17403192]
98. Murphy P, Koh D-M. Imaging in clinical trials. Cancer Imaging. 2010; 10:S74–S82. Spec no. [PubMed: 20880784]
99. Song HK, Dougherty L. Dynamic MRI with projection reconstruction and KWIC processing for simultaneous high spatial and temporal resolution. Magn Reson Med. 2004; 52(4):815–824. [PubMed: 15389936]
100. Kim JH, Lee JM, Park JH, et al. Solid pancreatic lesions: characterization by using timing bolus dynamic contrast-enhanced MR imaging assessment–a preliminary study. Radiology. 2013; 266(1):185–196. [PubMed: 23192779]
101. Konstantinidis IT, Do RKG, Gultekin DH, et al. Regional chemotherapy for unresectable intrahepatic cholangiocarcinoma: a potential role for dynamic magnetic resonance imaging as an imaging biomarker and a survival update from two prospective clinical trials. Ann Surg Oncol. 2014; 21(8):2675–2683. [PubMed: 24664624]
102. Sánchez-González, J.; Luna, A.; da Cruz, LC. Perfusion imaging by magnetic resonance. In: Luna, A.; Vilanova, JC.; da Cruz, LC., et al., editors. Functional imaging in oncology: biophysical basis and technical approaches. Vol. 1. Berlin: Springer; 2014. p. 341-376.
103. Cai W, Li F, Wang J, et al. A comparison of arterial spin labeling perfusion MRI and DCE-MRI in human prostate cancer. NMR Biomed. 2014; 27(7):817–825. [PubMed: 24809332]
104. Bazelaire, C De; Rofsky, NM.; Duhamel, G., et al. Arterial spin labeling blood flow magnetic resonance imaging for the characterization of metastatic renal cell carcinoma (1). Acad Radiol. 2005; 12(3):347–357. [PubMed: 15766695]
105. Aguirre-Reyes DF, Sotelo JA, Arab JP, et al. Intrahepatic portal vein blood volume estimated by non-contrast magnetic resonance imaging for the assessment of portal hypertension. Magn Reson Imaging. 2015; 33(8):970–977. [PubMed: 26117696]
106. Schraml C, Schwenzer NF, Martirosian P, et al. Perfusion imaging of the pancreas using an arterial spin labeling technique. J Magn Reson Imaging. 2008; 28(6):1459–1465. [PubMed: 19025955]
107. Luna A, Martin T, Alcala-Mata L, et al. Feasibility of arterial spin label to differentiate solid and cystic focal liver lesions. Scientific poster gastrointestinal (MR technique). RSNA. 2014 SSQ08–2.
108. ter Voert EG, Heijmen L, van Laarhoven HW, et al. In vivo magnetic resonance spectroscopy of liver tumors and metastases. World J Gastroenterol. 2011; 17(47):5133–5149. [PubMed: 22215937]
109. Kuo YT, Li CW, Chen CY, et al. In vivo proton magnetic resonance spectroscopy of large focal hepatic lesions and metabolite change of hepatocellular carcinoma before and after transcatheter

arterial chemoembolization using 3.0-T MR scanner. J Magn Reson Imaging. 2004; 19(5):598–604. [PubMed: 15112309]

110. Soper R, Himmelreich U, Painter D, et al. Pathology of hepatocellular carcinoma and its precursors using proton magnetic resonance spectroscopy and a statistical classification strategy. Pathology. 2002; 34(5):417–422. [PubMed: 12408339]
111. Fischbach F, Schirmer T, Thormann M, et al. Quantitative proton magnetic resonance spectroscopy of the normal liver and malignant hepatic lesions at 3.0 Tesla. Eur Radiol. 2008; 18(11):2549–2558. [PubMed: 18491103]
112. Xu L, Liu B, Huang Y, et al. 3.0 T proton magnetic resonance spectroscopy of the liver: quantification of choline. World J Gastroenterol. 2013; 19(9):1472–1477. [PubMed: 23539666]
113. Van Beers BE, Daire JL, Garteiser P. New imaging techniques for liver diseases. J Hepatol. 2015; 62(3):690–700. [PubMed: 25457198]
114. Chen L, Zhang J, Zhang L, et al. Meta-analysis of gadoxetic acid disodium (Gd-EOB-DTPA)-enhanced magnetic resonance imaging for the detection of liver metastases. PLoS One. 2012; 7(11):e48681. [PubMed: 23144927]
115. Park Y, Kim SH, Kim SH, et al. Gadoxetic acid (Gd-EOB-DTPA)-enhanced MRI versus gadobenate dimeglumine (Gd-BOPTA)-enhanced MRI for preoperatively detecting hepatocellular carcinoma: an initial experience. Korean J Radiol. 2010; 11(4):433–440. [PubMed: 20592927]
116. Marin D, Di Martino M, Guerrisi A, et al. Hepatocellular carcinoma in patients with cirrhosis: qualitative comparison of gadobenate dimeglumine-enhanced MR imaging and multiphasic 64-section CT. Radiology. 2009; 251(1):85–95. [PubMed: 19332848]
117. Grazioli L, Morana G, Kirchin MA, et al. Accurate differentiation of focal nodular hyperplasia from hepatic adenoma at gadobenate dimeglumine-enhanced MR imaging: prospective study. Radiology. 2005; 236(1):166–177. [PubMed: 15955857]
118. Grazioli L, Bondioni MP, Haradome H, et al. Hepatocellular adenoma and focal nodular hyperplasia: value of gadoxetic acid-enhanced MR imaging in differential diagnosis. Radiology. 2012; 262(2):520–529. [PubMed: 22282184]
119. Soulez G, Bloomgarden DC, Rofsky NM, et al. Prospective cohort study of nephrogenic systemic fibrosis in patients with stage 3–5 chronic kidney disease undergoing MRI with injected gadobenate dimeglumine or gadoteridol. AJR Am J Roentgenol. 2015; 205(3):469–478. [PubMed: 26295633]
120. Nandwana SB, Moreno CC, Osipow MT, et al. Gadobenate dimeglumine administration and nephrogenic systemic fibrosis: Is there a real risk in patients with impaired renal function? Radiology. 2015; 276(3):741–747. [PubMed: 25875973]

KEY POINTS

- MR imaging provides different multiple imaging biomarkers for the assessment of hepatobiliary and pancreatic malignancies, which can be integrated in a comprehensive protocol using a multiparametric approach.
- Diffusion-weighted imaging is now fully embedded in clinical protocols in the evaluation of abdominal malignancies.
- Perfusion MR imaging is technically ready for the clinical arena, with a promising role in the assessment of response to targeted-therapies.
- Magnetic resonance (MR) elastography and ^{1}H-MR spectroscopy can be used to assess focal liver lesions, but are still limited to research centers.
- Hepatobiliary contrast agents are widely used in the detection of metastasis and in the assessment of hepatocellular carcinoma.

Box 1

Scanning parameters to optimize in diffusion-weighted imaging acquisitions

Increase SNR

Maintain TE as shortest as possible

Coarse matrix

Use parallel imaging

Simultaneous gradient application

Multiple signal averaging

Reduce artifacts

Optimize fat suppression

Increase bandwidth

Control eddy currents

Avoid areas with susceptibility artifacts

Use respiratory synchronism techniques

Box 2

Main characteristics of breath-hold and free-breathing diffusion-weighted sequences

Breath-hold sequence
Limited SNR, spatial resolution, and slice thickness
Prone to distortion and ghosting artifacts
Limited number of b values (usually 2 or 3)
Limited quality of ADC map due to misregistration
Shorter acquisition time
Free breathing sequence
Increased SNR, spatial resolution, and slice thickness
Prone to respiratory artifacts, blurring, and volume averaging
Permit to acquire more b values
Better quality of ADC map
Usually longer acquisition time

Box 3

Classification of pancreatic cystic lesions

Benign cystic tumors

Serous cystadenoma

Cystic tumors with malignant potential

Mucinous cystic neoplasms (MCN)

Intraductal papillary mucinous neoplasm (IPMN)

Frankly malignant cystic tumors

Cystadenocarcinoma

Intraductal papillary mucinous adenocarcinoma (Malignant IPMN)

Cystic-appearing pancreatic tumors

Solid pseudopapillary neoplasm

Acinar cell cystadenocarcinoma

Lymphangioma

Hemangioma

Paraganglioma

Solid pancreatic lesions with cystic degeneration

Pancreatic adenocarcinoma

Cystic pancreatic neuroendocrine neoplasm (PNET)

Metastasis

Cystic teratoma

Sarcoma

Nonneoplastic cystic lesions

True epithelial cyst

Mucinous nonneoplastic cyst

Pseudocyst

Abscess

Box 4

Goals of an ideal perfusion MR imaging examination

1. High temporal resolution: To capture ultrafast changes in contrast concentration in the tissue of interest
2. High spatial resolution: To detect very small lesions (<1 cm in size)
3. Complete volumetric coverage of the organ of interest
4. Methods to account for respiratory motion

Box 5

^{1}H-MR spectroscopy for liver tumor assessment

Techniques

Stimulated-echo acquisition mode (STEAM)

- Better definition of voxel
- Shorter minimum TE

Point-resolved spectroscopy (PRESS)

- Double SNR than STEAM

Sequence design

3T magnet is preferred

Torso phased-array coil

Automatic or manual shimming

Single-voxel (10–30 mm^2) technique: Only a focal area of tissue is explored

Adequate positioning of voxel is critical to avoiding large vessel and areas of tumor necrosis

Acquisition with water suppression and without fat suppression

Respiratory motion synchronism or postprocessing correction

Shortcomings

Prone to field inhomogeneities

Prone to motion and other artifacts

Limited spectral resolution

Complex acquisition and postprocessing

Needs of T1 and T2 corrections

Limited clinical experience

Box 6

Typical MR imaging characteristics of common solid benign and malignant focal liver lesions with hepatobiliary contrast agent

Focal nodular hyperplasia

Isointense to hypointense on T1-weighted images

Isointense to hyperintense on T2-weighted images

Intense arterial enhancement and isointense to hyperintense to liver in portal venous phase

Isointense to hyperintense to liver in HB phase

Central scar in 80%, which is hyperintense on T2-weighted sequence and shows delayed enhancement

Hepatocellular adenoma

Isointense to hyperintense with heterogeneous appearance on T1-weighted images

Variable signal intensity on T2-weighted images

Intense arterial enhancement

Absence of enhancement in HB phase, although in some cases can show variable enhancement with gadoxetic acid

Fat and hemorrhage can be present

Hepatocellular carcinoma

Variable appearance on T1-weighted images

Isointense to hyperintense on T2-weighted images

Intense arterial enhancement and washout to liver in portal/delayed phases

Hypointense to liver in HB phase, although well-differentiated lesions can show enhancement

Hypovascular HCC cannot show intense arterial enhancement

Metastasis

Variable appearance on T1-weighted images

Isointense to hyperintense on T2-weighted images

Variable appearance on dynamic series, hypervascular to hypovascular on arterial phase, with washout in portal venous phase. Similar behavior to primary tumor on DCE-MR imaging

Absence of enhancement in HB phase

Modified from Lebedis C, Luna A, Soto JA. Use of magnetic resonance imaging contrast agents in the liver and biliary tract. Magn Reson Imaging Clin N Am 2012;20(4):715–37.

Box 7

Main clinical applications of hepatobiliary contrast agents in the assessment of focal liver lesions

Improved detection of colorectal cancer liver metastasis

- HBCAs have shown improved sensitivity and specificity than ultrasound, CT, and PET in the detection of liver metastasis
- These results are improved if they are used in combination with DWI
- In a recent meta-analysis including 1900 cases evaluating the detection of liver metastases, the sensitivity and specificity of gadoxetic acid were 93% and 95%, respectively[114]
- A recent consensus paper from a multidisciplinary expert panel stated that preoperative imaging with gadoxetic acid is of special interest in the assessment of patients with colorectal liver metastases who are going to be treated with chemotherapy[15]

Differentiation of FNH from adenoma

- Pooled sensitivities and specificities on this task are more than 83% and 95%, respectively, with both HBCAs[117,118]

Improved detection of HCC

- HBCAs improve diagnostic accuracy and sensitivity in the detection of HCC compared with multiphase CT
- HBCAs improves the detection of small HCC (<1 cm) compared with extracellular contrast agents according to preliminary results, although larger studies are needed to support these data
- According to initial data, the lesser the contrast enhancement during the HB phase, the higher the HCC aggressiveness
- Although dysplastic nodules mostly show enhancement on HB phase and not early HCC, there are not enough data to support the use of HBCAs for this task
- The role of HBCAs in the assessment of HCC and in its screening in cirrhotic livers has still to be defined and supported with cost-effectiveness studies or outcomes
- Hypointense nodules on HB phase, but with atypical enhancement pattern on DCE acquisition, should be considered suspicious for HCC and biopsy, or close surveillance is recommended

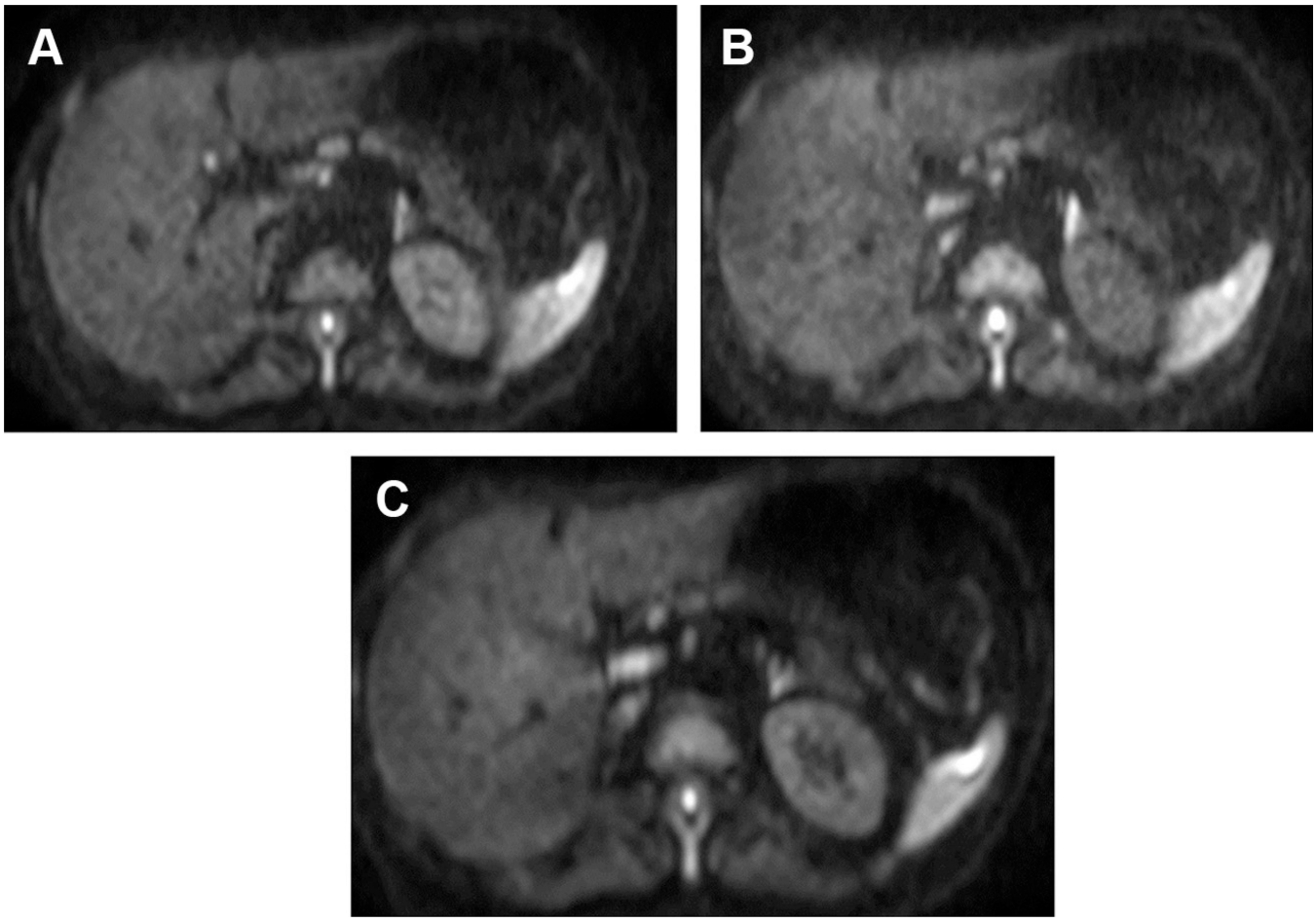

Fig. 1.

Techniques of respiratory synchronization in DWI of the liver. Notice different SNR and acquisition time in (*A*) breath-hold (acquisition time: 120 seconds; 20 seconds per breath-hold), (*B*) free-breathing (acquisition time: 80 seconds), and (*C*) respiratory trigger (acquisition time: 220 seconds) acquisitions.

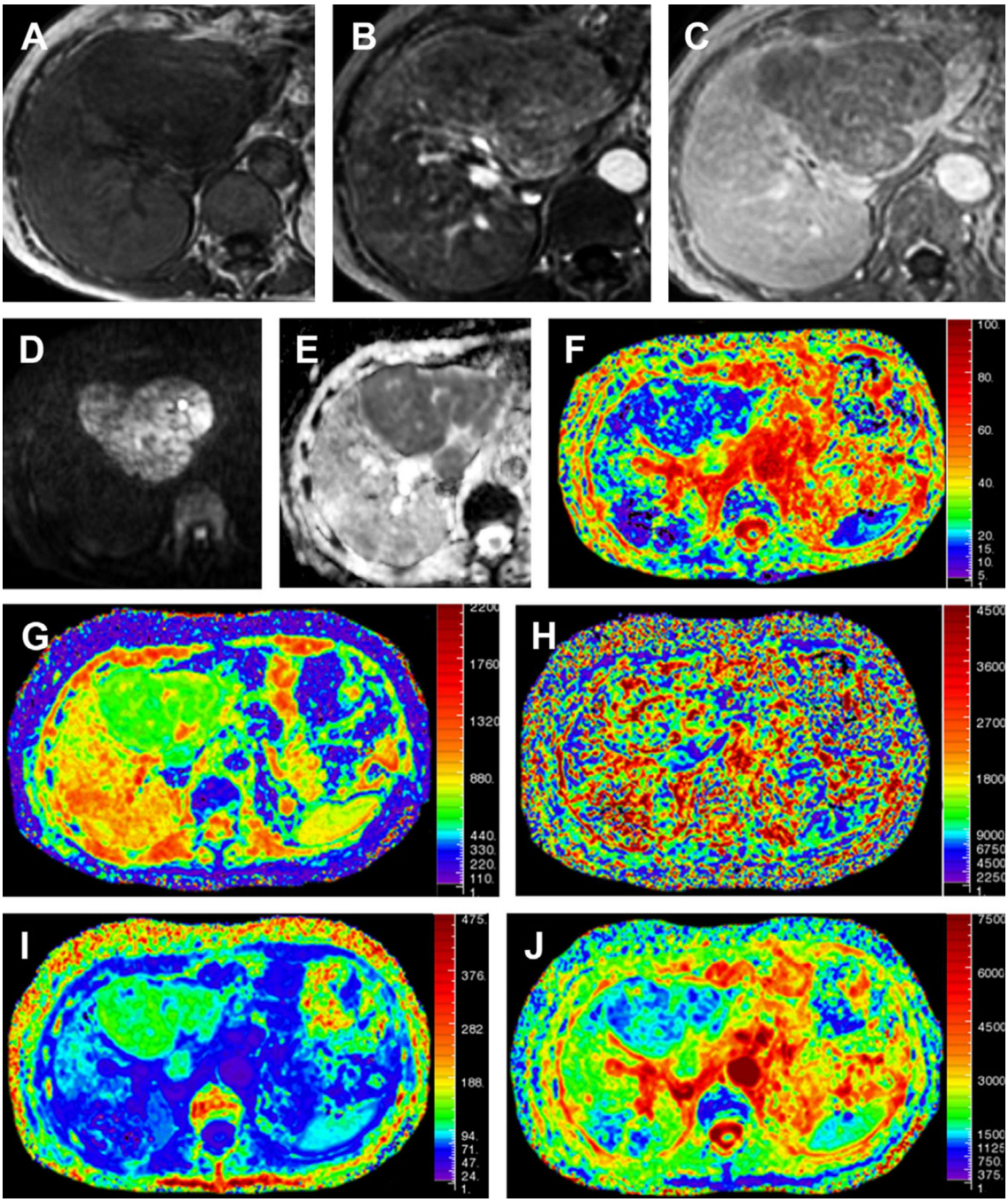

Fig. 2.

DWI of HCC analyzed with different models of signal decay. (*A*–*C*) Precontrast, arterial, and venous phases of DCE-MR imaging show a large focal liver lesion with heterogeneous wash-in during arterial phase and posterior washout. (*D*) DWI with b value of 2000 s/mm^2 shows high SI of the lesion and (*E*) very low ADC value (0.65 × 10^{-3} mm^2/s). IVIM model confirms the restriction of water diffusion of the lesion in the (*F*) D map with a value of 0.6 × 10^{-3} mm^2/s. (*G*) Increased perfusion fraction (16%) and (*H*) pseudodiffusion value (D*:

28.8 × 10^{-3} mm^2/s) demonstrate increased flow within the nodule. (*I, J*) Derived parameters from DKI show a kurtosis value of 1.1 and mean diffusion kurtosis of 1.4 × 10^{-3} mm^2/s.

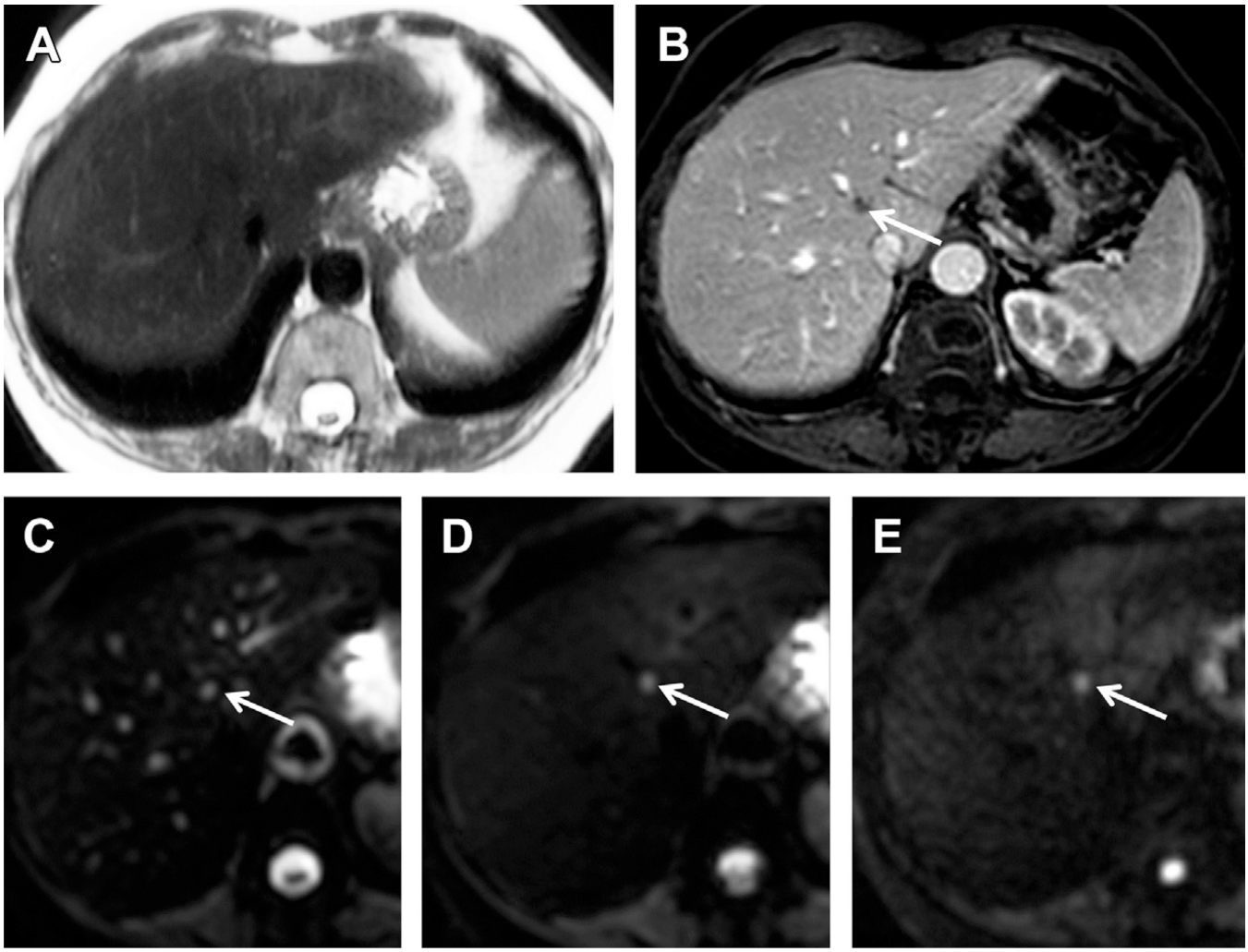

Fig. 3.

Breast cancer liver metastasis (*arrows*) detection. (*A*) Axial turbo spin-echo (TSE) T2-weighted sequence does not depict a lesion in segment IVa, which was hardly visualized in (*B*) postcontrast portal phase of DCE-MR imaging sequence (*arrow*). (*C–E*) Axial DWI with b values of 0, 50 and 900 s/mm^2: notice how the lesion is better visualized (*arrows*) against a background liver parenchyma without vessel signal with b value of 50 s/mm^2. High SI on high b-value image suggests its malignant origin.

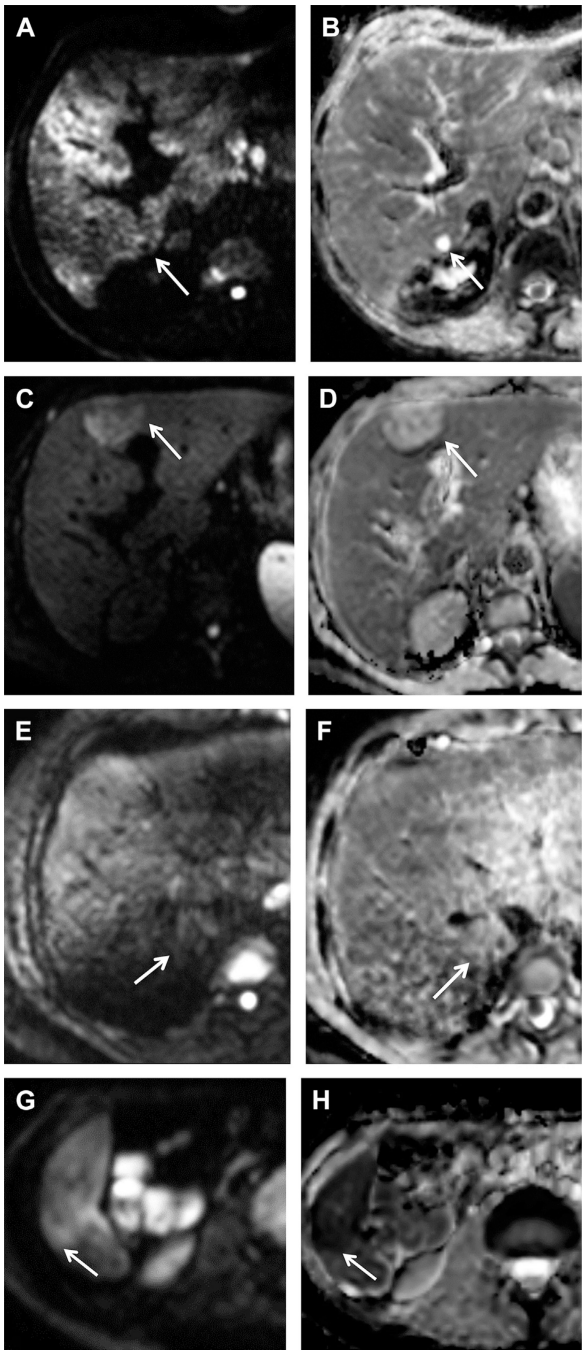

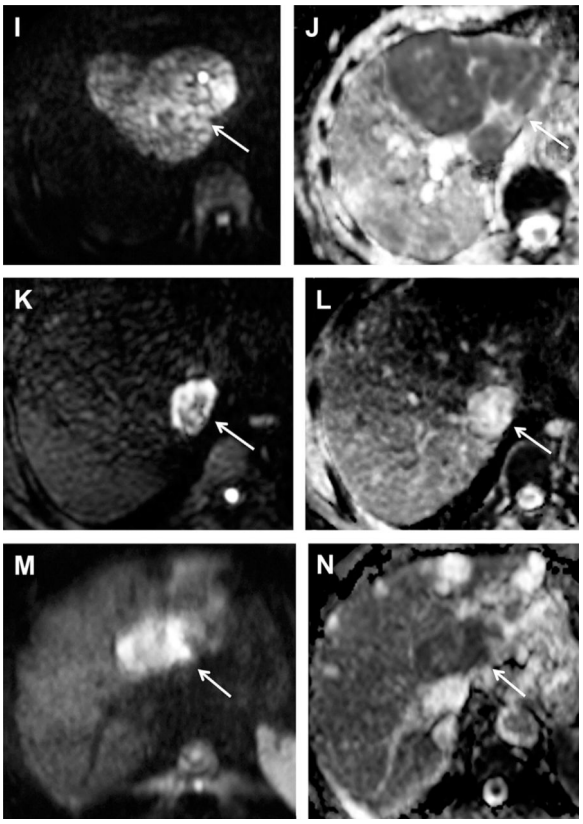

Fig. 4.

Typical behavior on DWI of the most common focal liver lesions (*arrows*). Paired high b-value image and corresponding ADC map of (*A, B*) Simplecyst: ADC value: 2.1 × 10^{-3}mm^2/s. (*C, D*) Hemangioma: ADC value:1.4 × 10^{-3}mm^2/s. (*E, F*) FNH ADC value: 1.5 × 10^{-3} mm^2/s. (*G, H*) Hepatocellular adenoma: ADC value: 0.9 × 10^{-3} mm^2/s. (*I, J*) HCC: ADC value: 0.65 × 10^{-3} mm^2/s. (*K, L*) Colorectal liver metastasis: ADC value: 0.8 × 10^{-3} mm^2/s. (*M, N*) CHC: ADC value: 0.9 × 10^{-3} mm^2/s. Notice the overlap in ADC values between benign and malignant solid lesions.

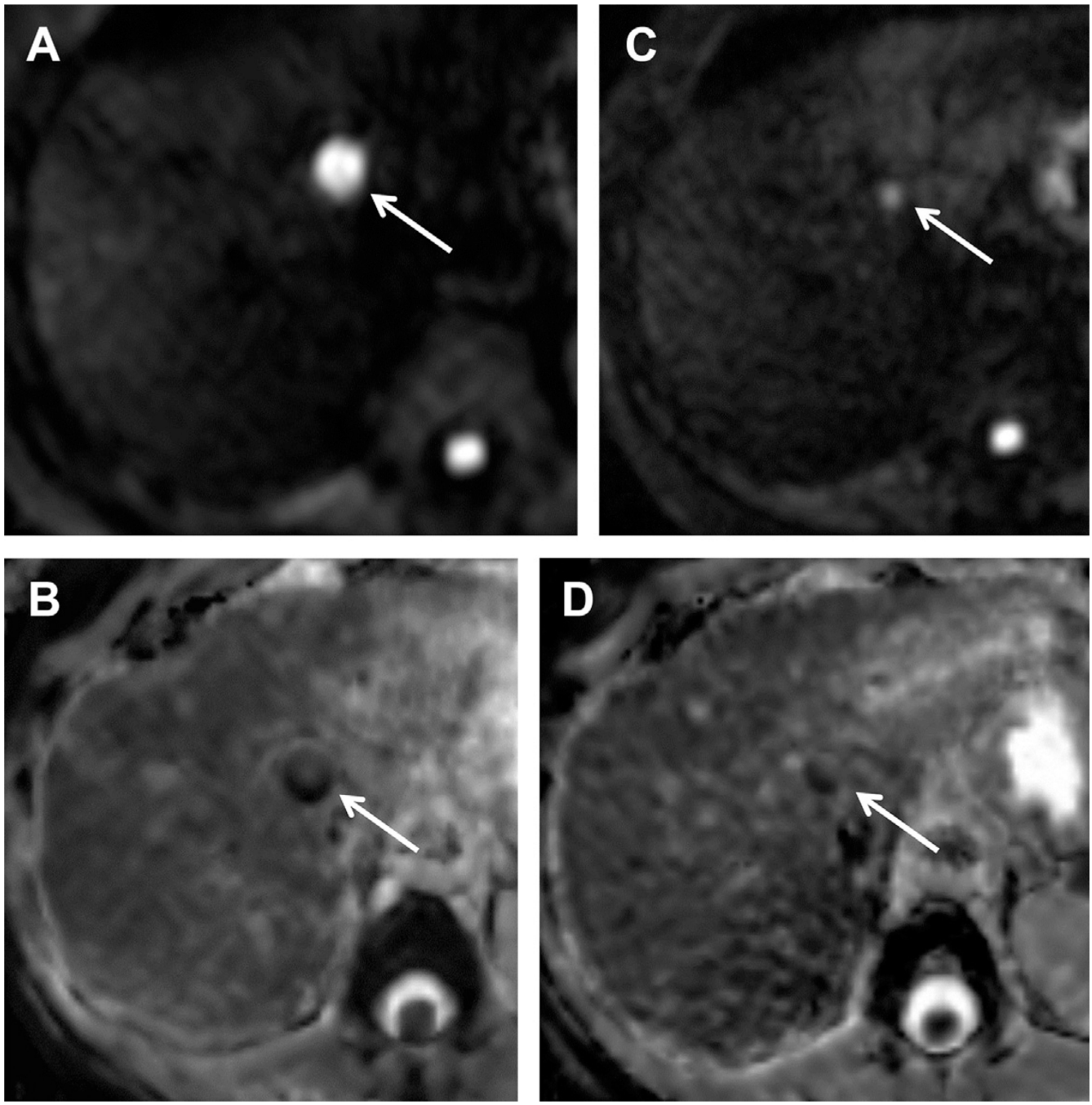

Fig. 5.

Therapy monitoring of breast cancer liver metastasis (*arrows*) with DWI. (*A, B*) Pretreatment DWI with b value of 900 s/mm^2 and corresponding ADC map show lesions with true restriction of water motion in segment IVa. ADC value: 0.48 × 10^{-3} mm^2/s. (*C, D*) 4 months after chemotherapy DWI and ADC map demonstrate partial response with decrease in size and in SI in high b-value image, with increase in ADC value up to 1.1 × 10^{-3} mm^2/s.

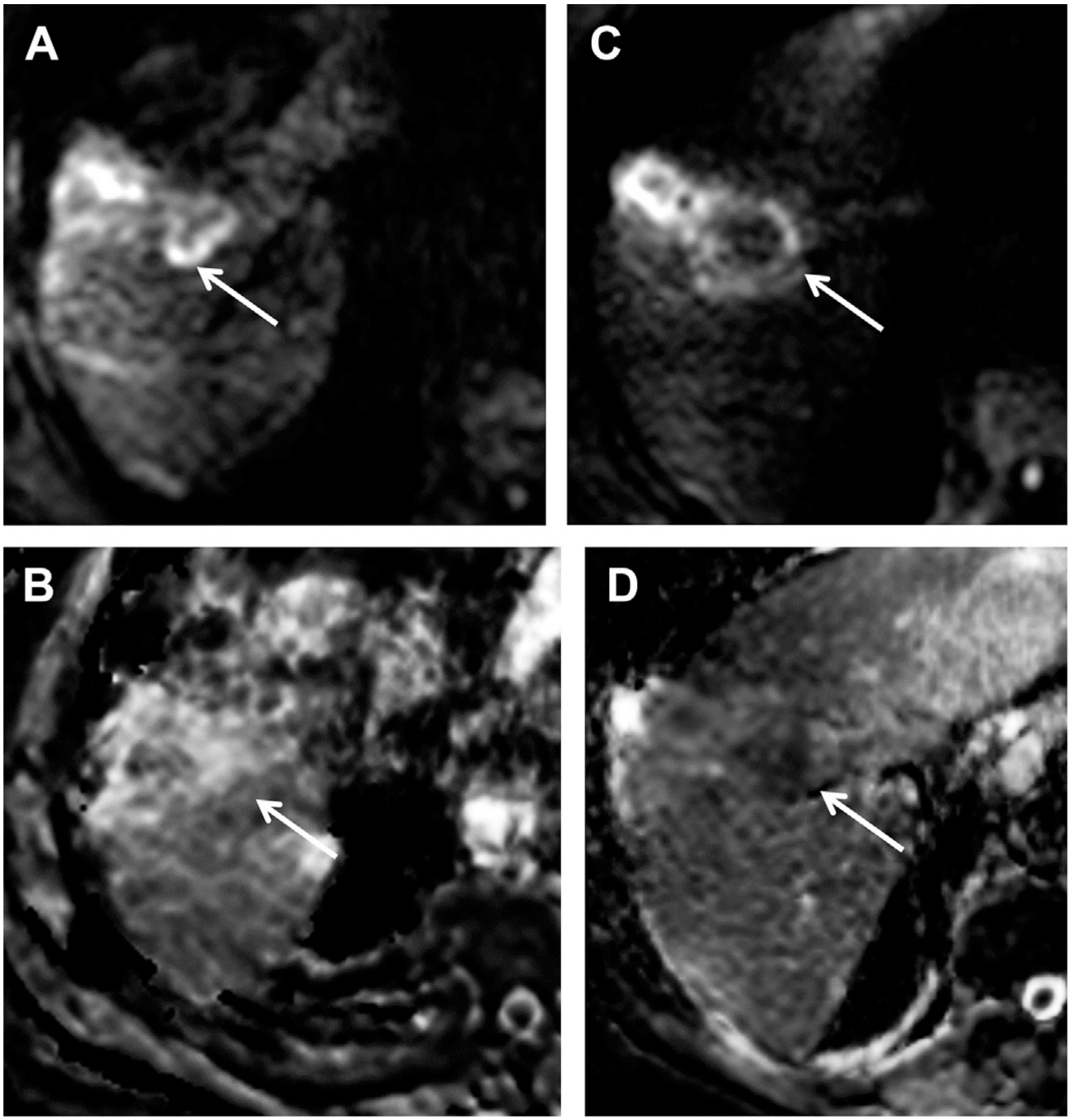

Fig. 6.

Therapy monitoring of colorectal cancer liver metastasis (*arrows*) with DWI. (*A, B*) Pretreatment DWI with b value of 900 s/mm^2 and corresponding ADC map show a lesion with heterogeneous restriction of water motion in segment VIII. High pretreatment ADC value of 1.5×10^{-3} mm^2/s suggests poor response to treatment. (*C, D*) 8 months after chemotherapy DWI and ADC map demonstrate progression with increase in size and in SI on high b-value image and decrease in ADC value: 0.73×10^{-3} mm^2/s.

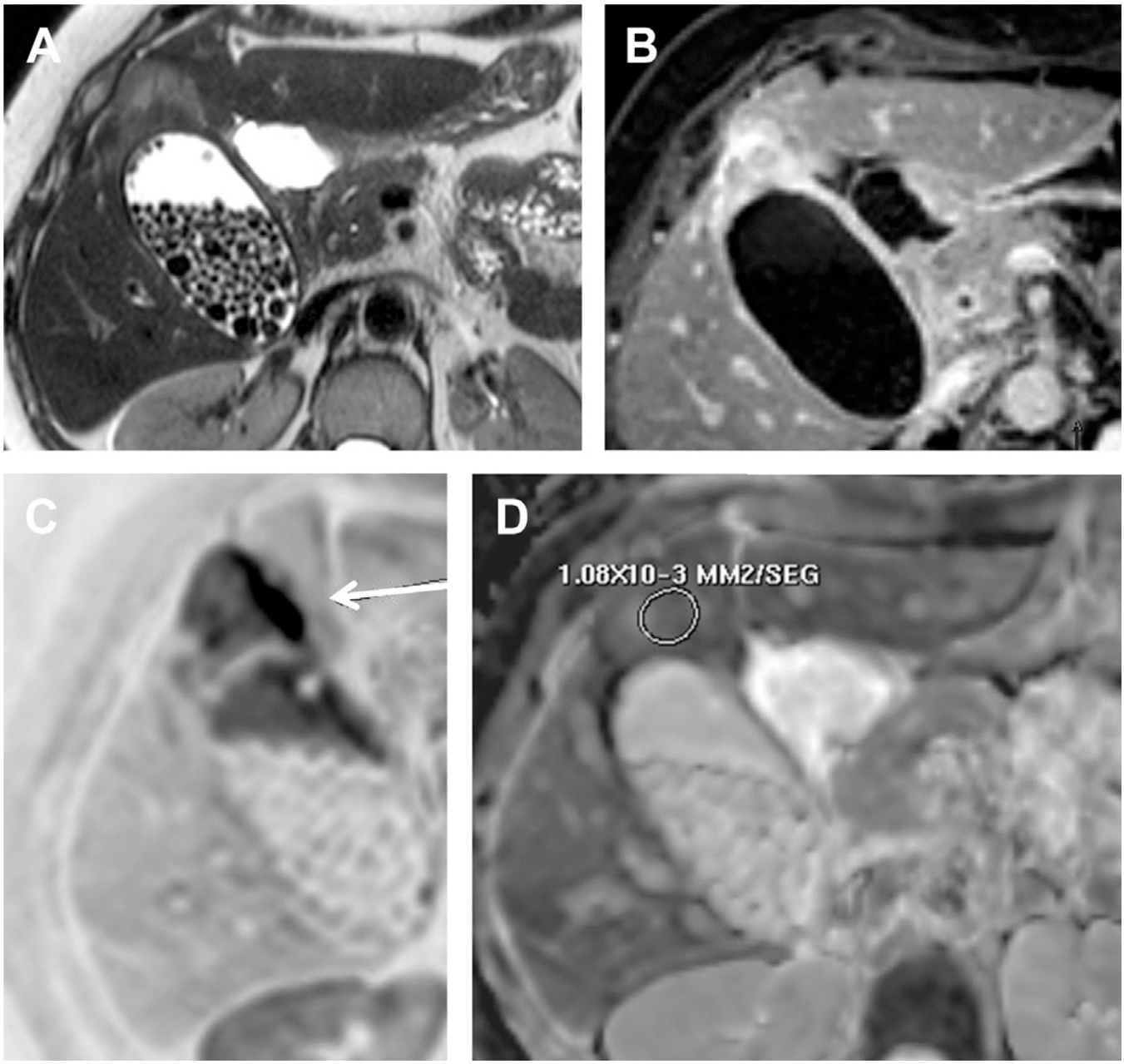

Fig. 7.

Gallbladder carcinoma with DWI. (*A*) Axial TSE T2-weighted image and (*B*) delayed postcontrast T1 high resolution isotropic volume excitation (THRIVE) show a mural thickening of the fundus of the gallbladder invading the adjacent hepatic parenchyma. Notice the presence of multiple lithiasis. (*C, D*) High b-value DWI with inverted gray-scale and corresponding ADC map demonstrates restriction of water motion of the mural lesion (*arrow*), with low ADC of 1.08×10^{-3} mm^2/s (ROI).

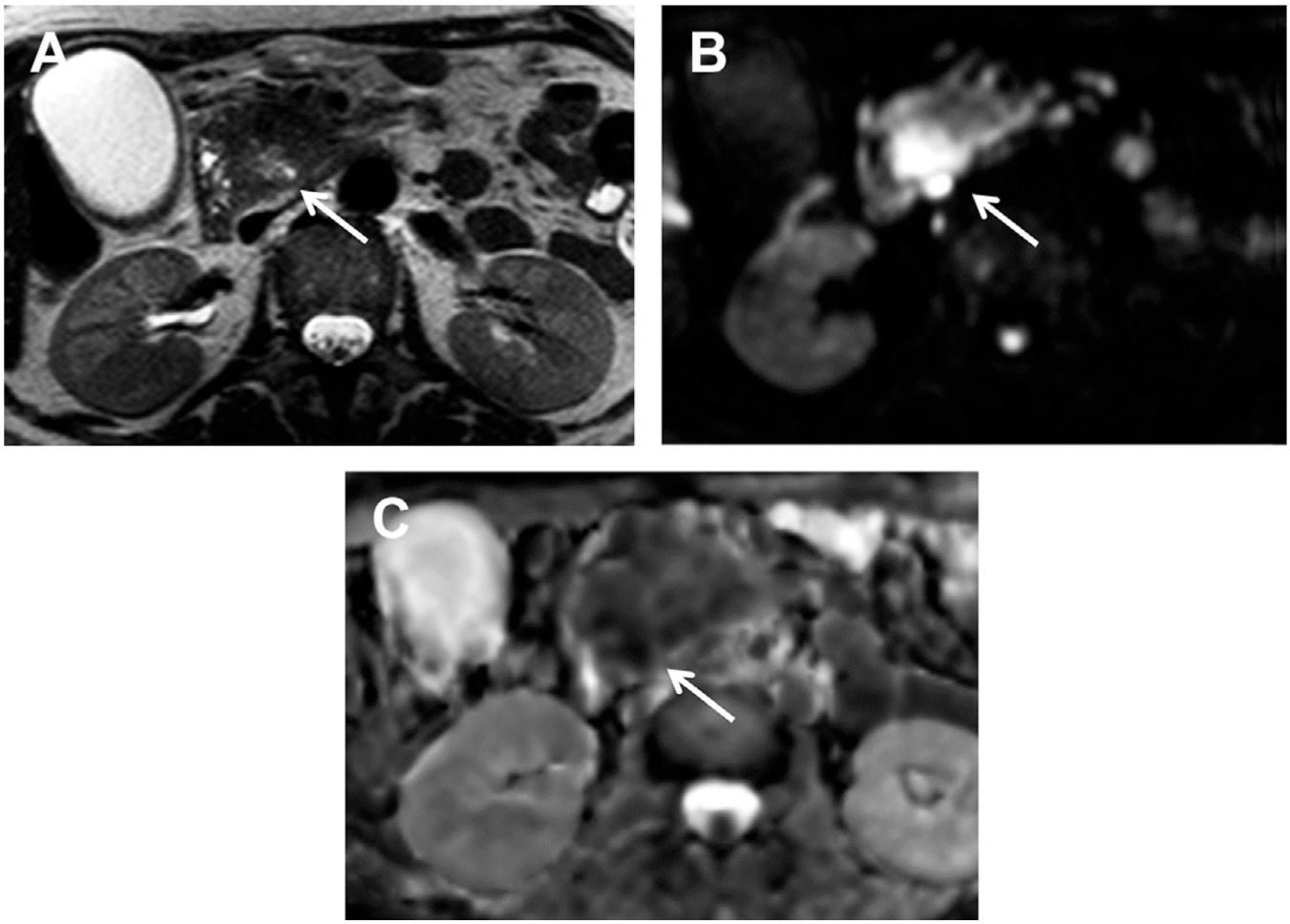

Fig. 8.

Pancreatic carcinoma (*arrows*) with DWI. (*A*) Axial TSE T2-weighted image shows an ill-defined mass located in the pancreatic head. (*B, C*) High b-value DWI and corresponding ADC map demonstrate restriction of water motion of the lesion, with low ADC value: 0.9×10^{-3} mm^2/s.

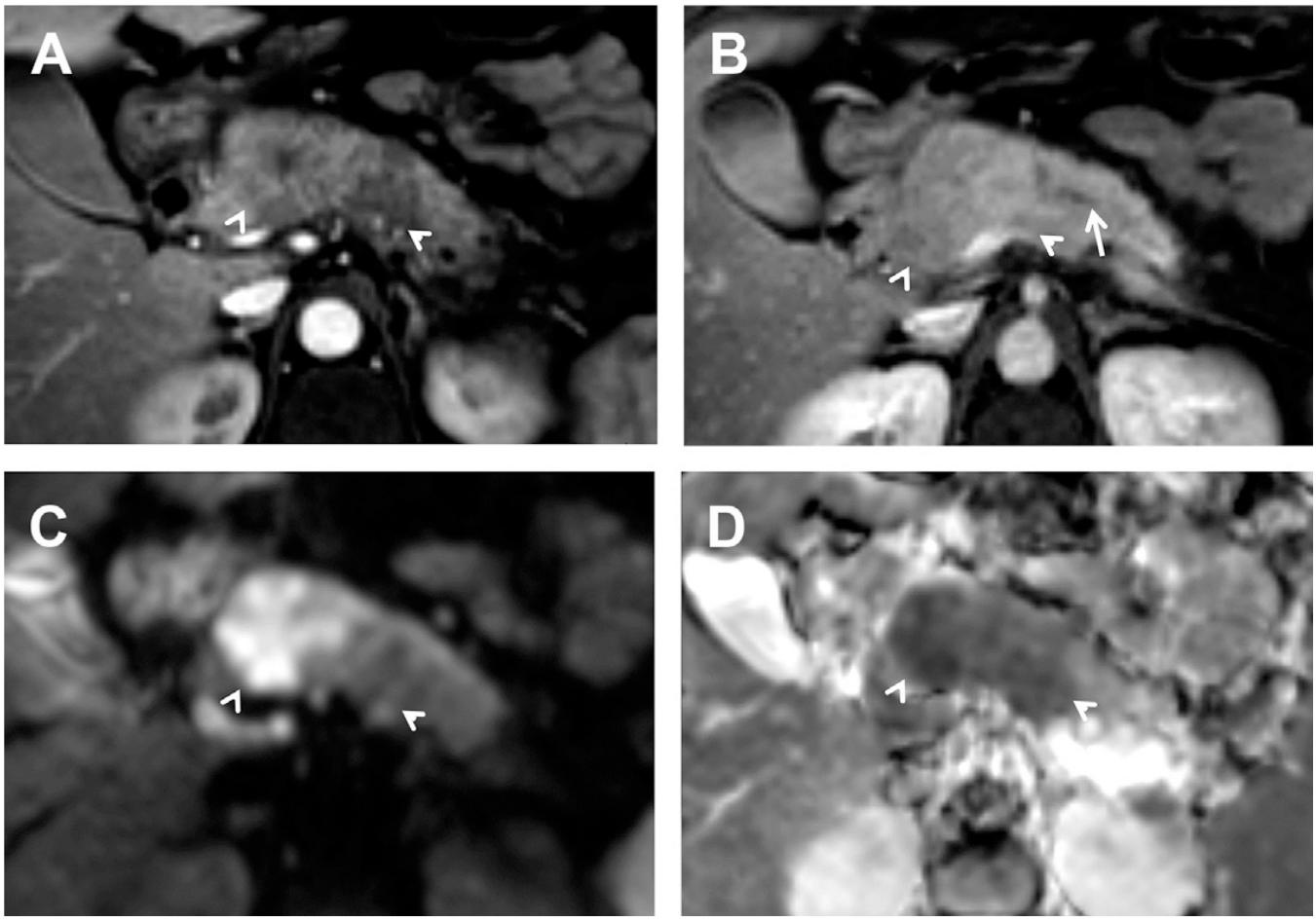

Fig. 9.

Mass-forming chronic pancreatitis (*arrowheads*). (*A, B*) DCE-MR imaging during the portal and delayed phases show a large mass in the pancreatic head with peripheral enhancement during the portal phase and delayed heterogeneous wash-in. Notice the distal dilatation of main pancreatic duct due to obstruction (*arrow*). (*C, D*) High b-value DWI and corresponding ADC map demonstrate restriction of water motion of the lesion. Notice how the limits of the lesion are better depicted on DWI compared with DCE-MR imaging.

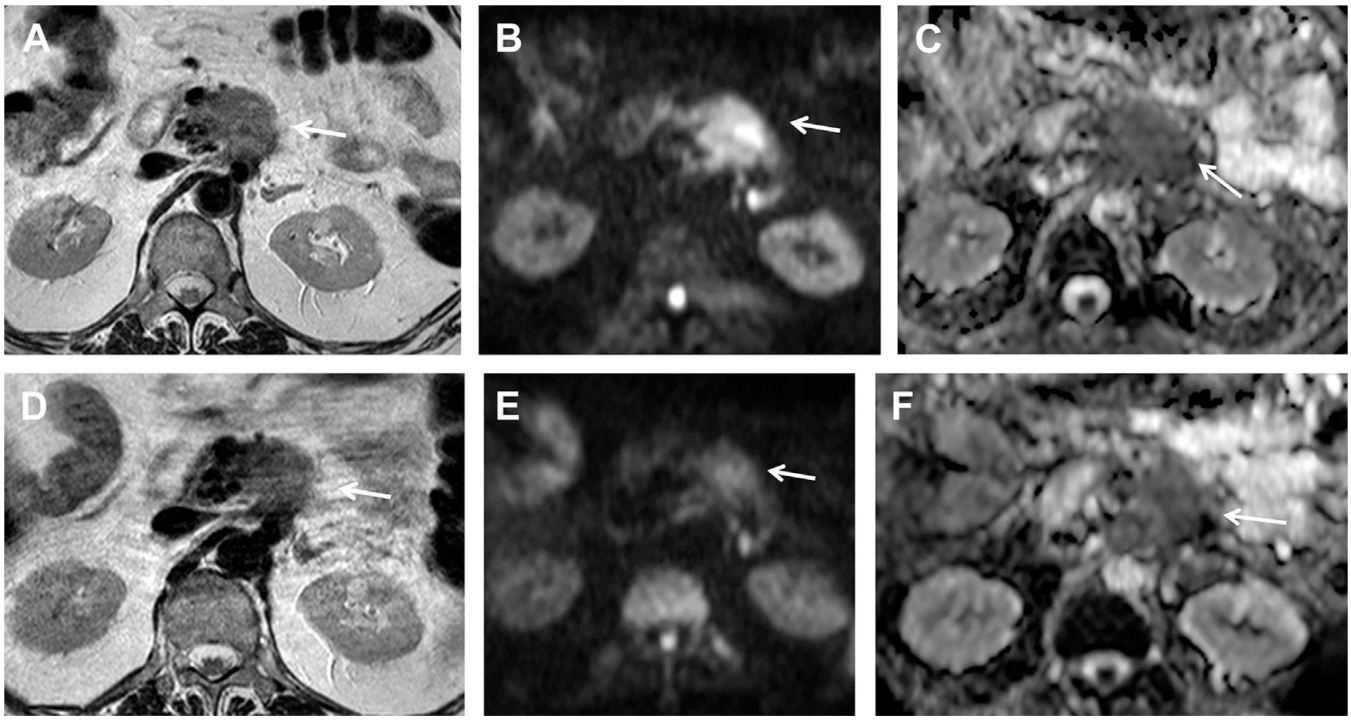

Fig. 10.

Therapy monitoring of pancreatic carcinoma (*arrows*) with DWI. (*A*) Pretreatment axial TSE T2-weighted image depicts a large hyperintense lesion involving the distal aspect of the body and tail of the pancreas. (*B, C*) Pretreatment DWI with b value of 1000 s/mm^2 and corresponding ADC map show restriction of water motion of the pancreatic tumor with ADC value of 1.4×10^{-3} mm^2/s. (*D–F*) 5 months after chemotherapy TSE T2-weighted, DWI, and ADC map, respectively, demonstrate stable size of the mass, but with decrease in SI on high b-value image and increase in ADC value: 1.8×10^{-3} mm^2/s, indicating partial response.

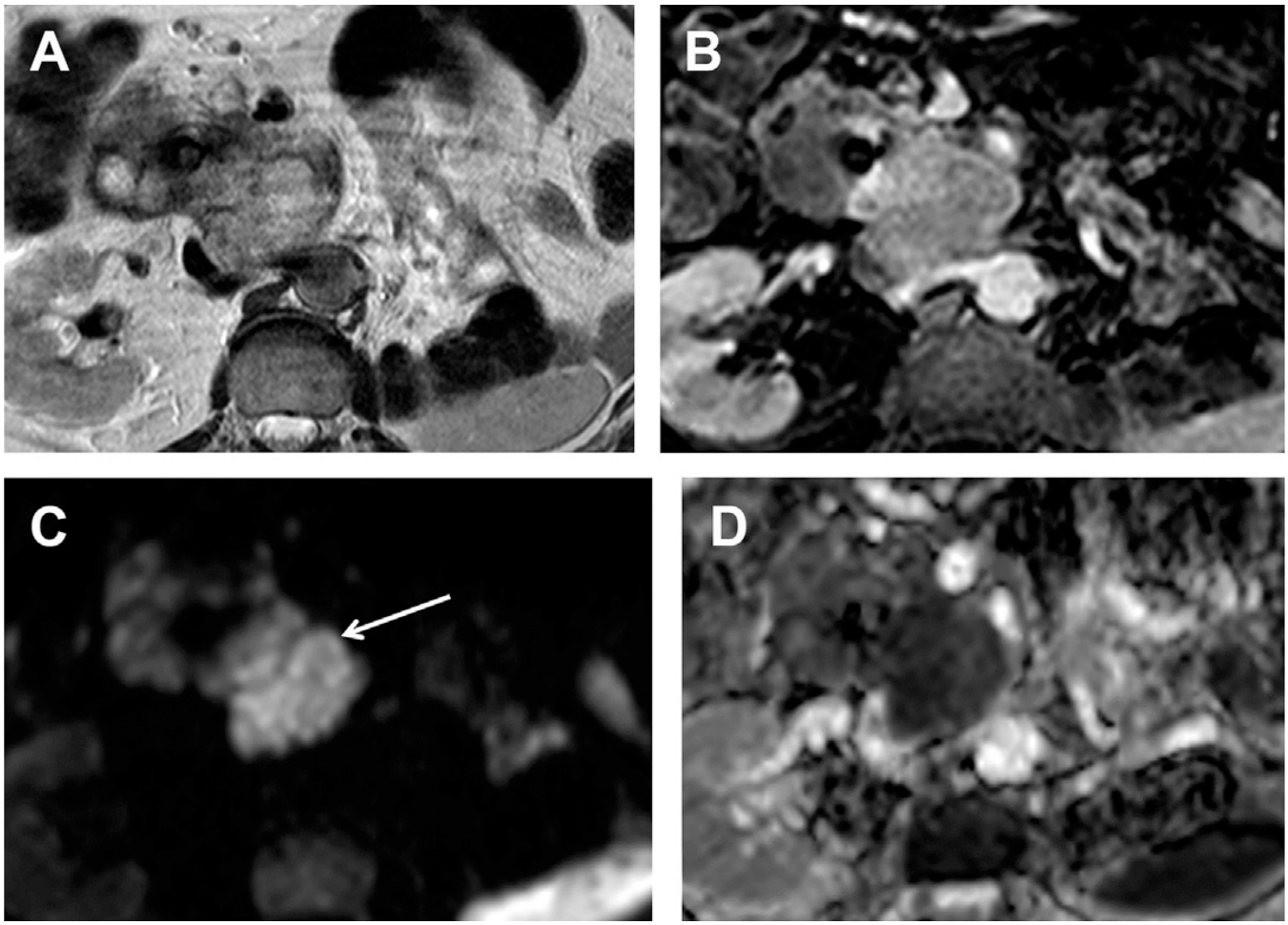

Fig. 11.

PNET. (*A*) Axial TSE T2-weighted and (*B*) postcontrast e-THRIVE during the arterial phase demonstrate a large mass in pancreatic head with vessel involvement. The mass shows high SI on T2-weighted image and intense heterogeneous enhancement. (*C, D*) DWI with b value of 800 s/mm^2 (*arrow*) and corresponding ADC map confirm the aggressiveness of the lesion with intense restriction of water motion (ADC: 1×10^{-3} mm^2/s).

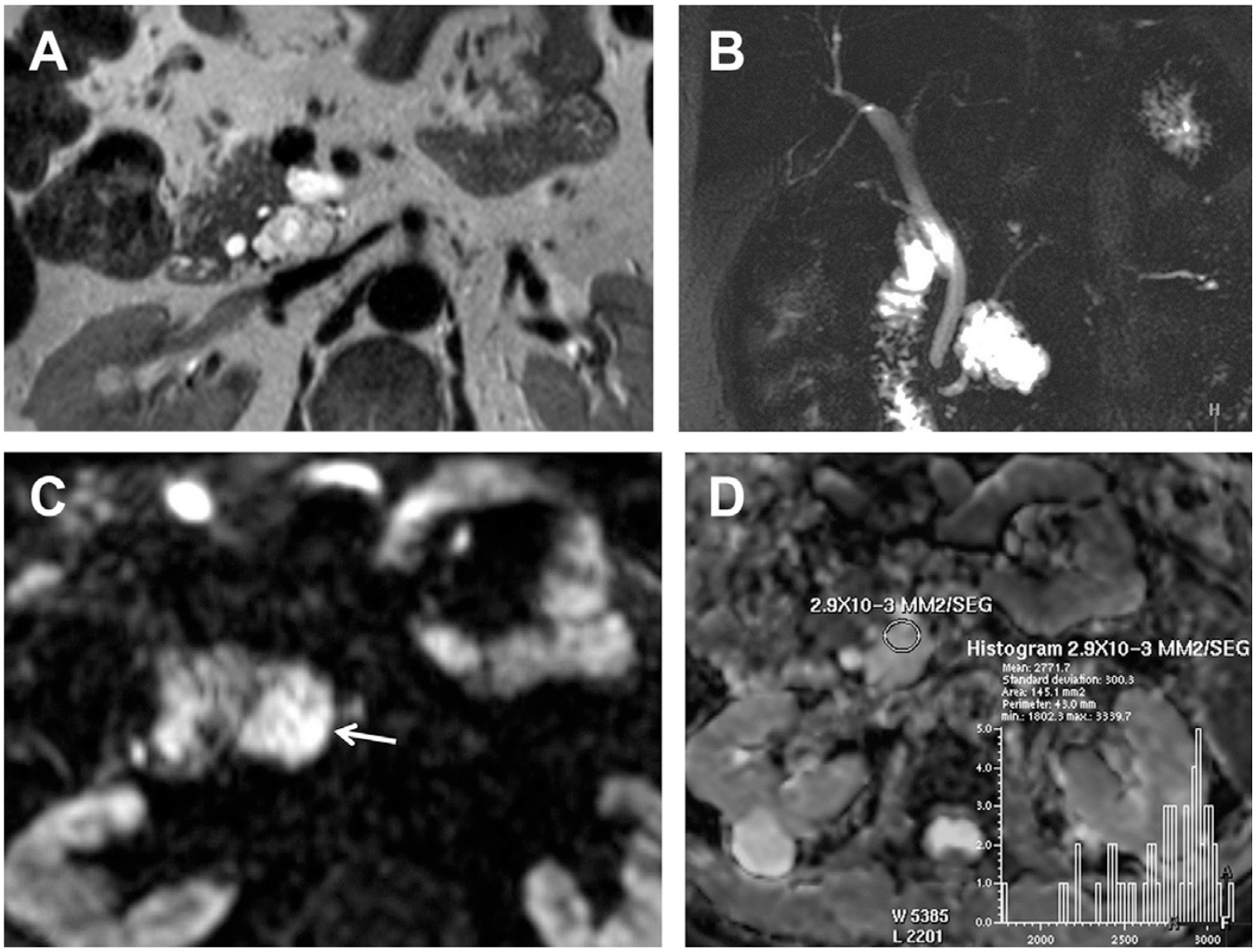

Fig. 12.

Accessory-branch IPMN. (*A, B*) Axial TSE T2-weighted and coronal thick-slice 2-dimensional cholangiography demonstrate a cystic mass with small locules and septa in the pancreatic head. The mass is connected to a secondary branch of the pancreatic duct. (*C, D*) DWI with b value of 800 s/mm^2 and corresponding ADC map show high signal on high b-value image (*arrow*), but absence of true restriction of water motion of the pancreatic tumor with ADC value of 2.9×10^{-3} mm^2/s (ROI). This appearance is due to T2 shine-through effect.

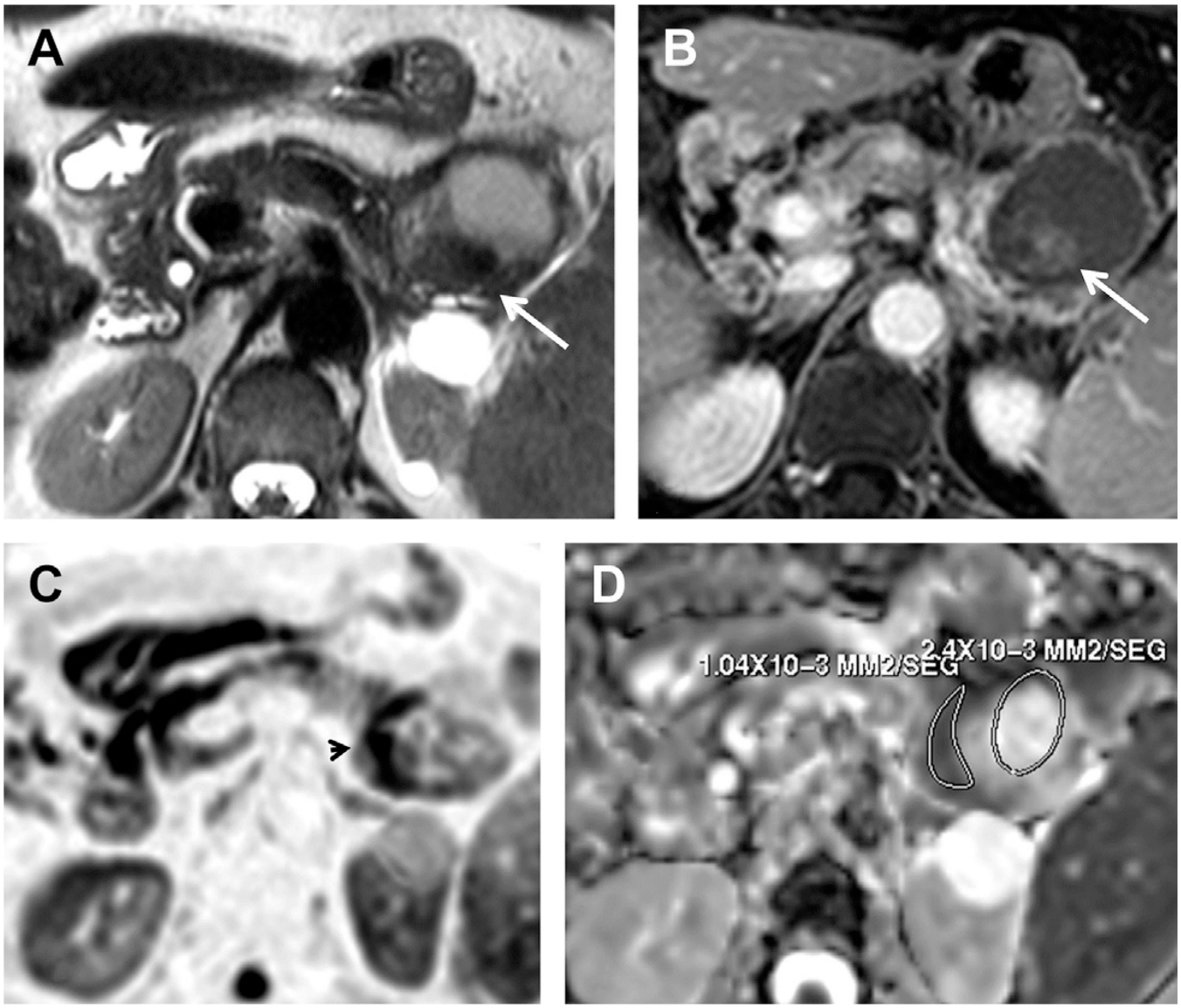

Fig. 13.

Malignant MCN. (*A, B*) Axial TSE T2-weighted image and (*B*) axial postcontrast THRIVE during the venous phase show a complex cystic lesion with solid peripheral neoplastic component that shows enhancement and a mural nodule (*arrows*). (*C, D*) Diffusion-weighted image (*b*: 800 mm^2/s) with inverted gray-scale and corresponding ADC map demonstrate restriction of water motion in the solid mural thickening (*arrowhead*), with ADC value of 1.04×10^{-3} mm^2/s. ADC of the cystic component is 2.4×10^{-3} mm^2/s (ROIs).

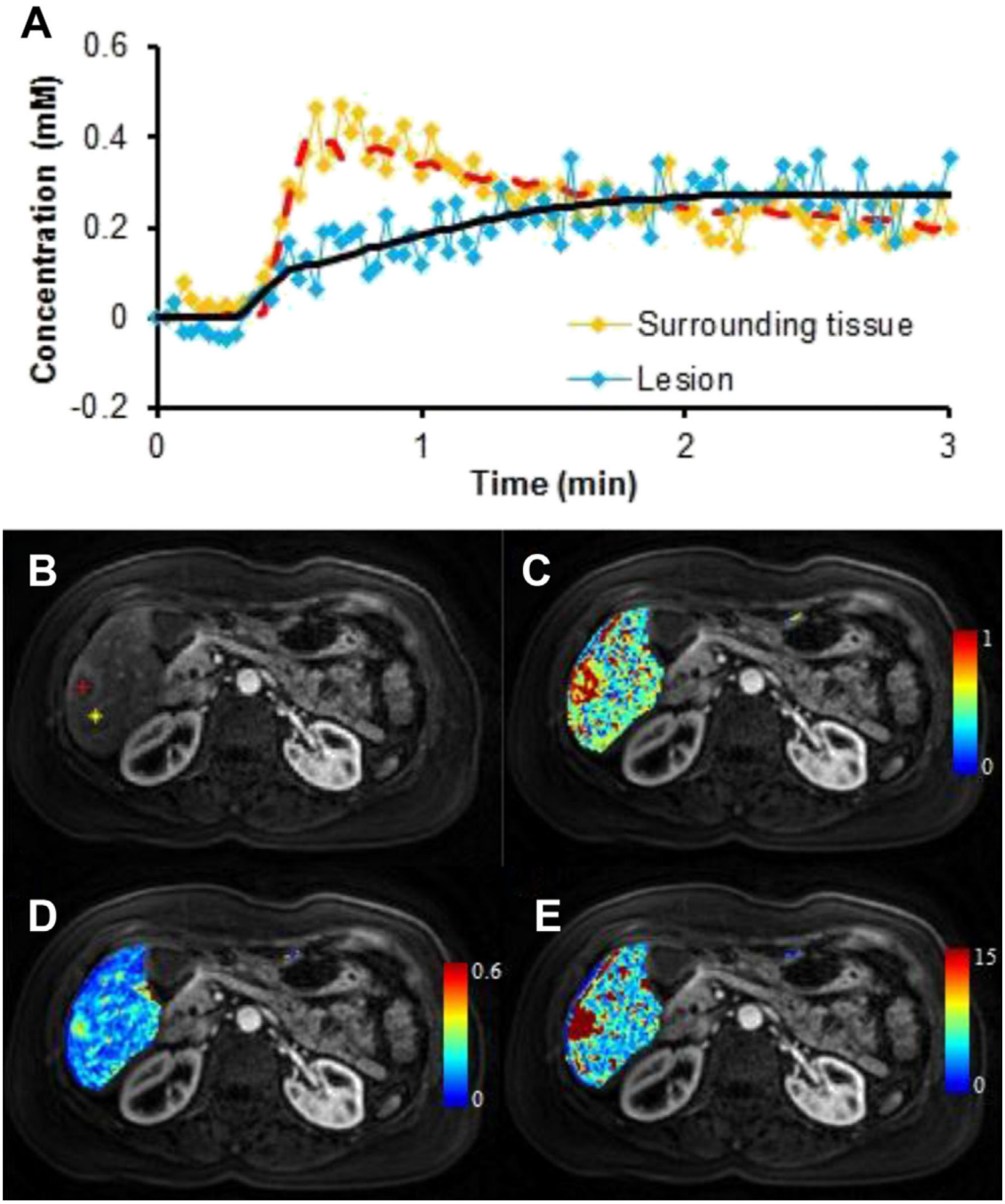

Fig. 14.

Perfusion modeling in a patient with metastatic adenocarcinoma using 3-dimensional through-time spiral GRAPPA (generalized autocalibrating partially parallel acquisitions) acceleration technique with a temporal resolution of 2 seconds (*A*). Representative concentration-time curves of both lesion and normal surrounding tissue as shown in the T_1-weighted image (*B*). Corresponding liver perfusion maps of (*C*) arterial fraction (AF) should appear arterial fraction (AF), (*D*) DV, and (*E*) MTT. The AF, DV, and MTT for the lesion

(76.3%, 29.7%, and 58.7 seconds, respectively) were different from surrounding normal liver parenchyma (35%, 12.6%, and 5.6 seconds, respectively).

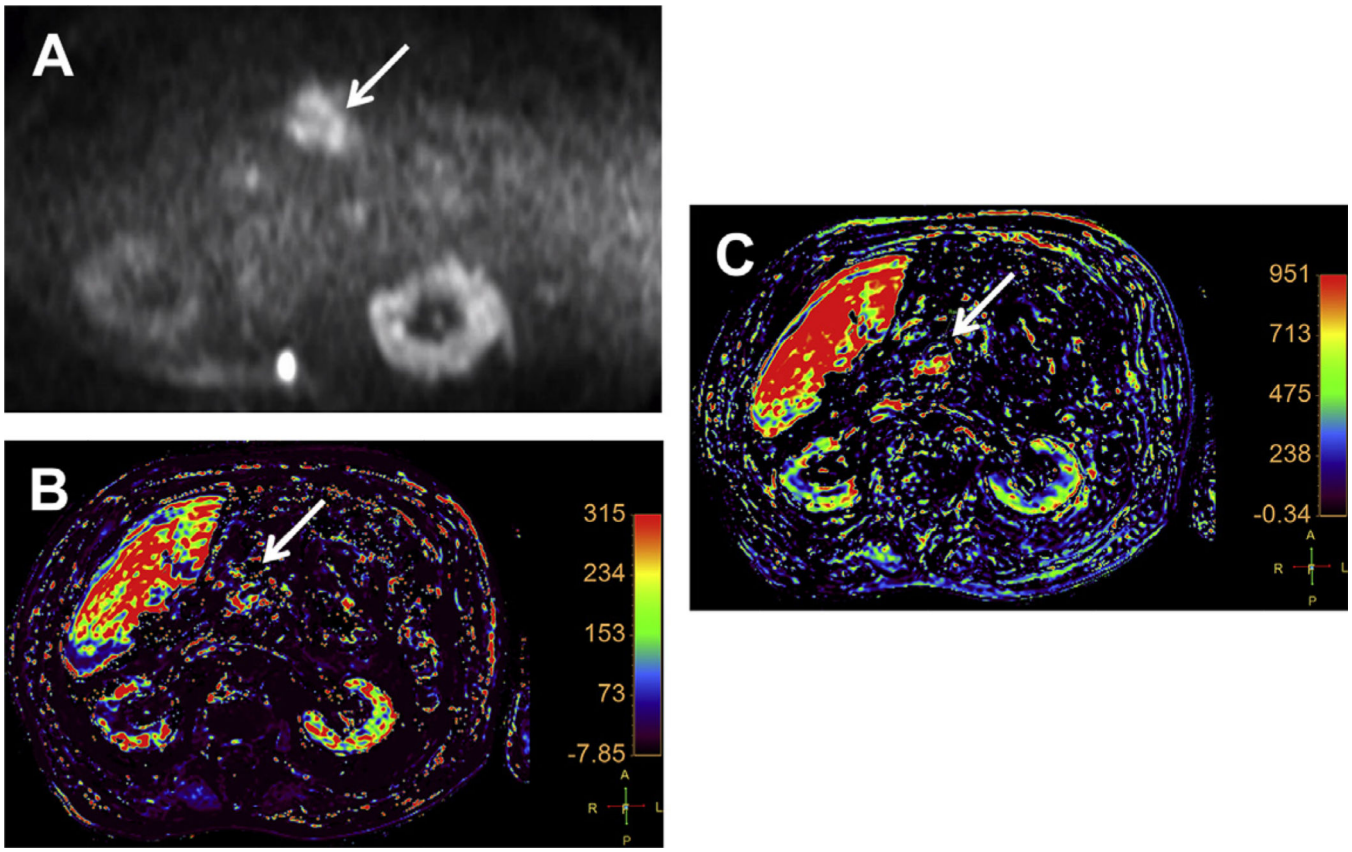

Fig. 15.

DCE-MR imaging in 79 year-old man with pancreatic cancer (*arrows*). (*A*) DWI with b value of 800 s/mm2 shows a pancreatic mass with high signal intensity. (*B, C*)K^{trans} and k_{ep} parametric maps respectively, obtained using a bicompartmental model from DCE-MR imaging, show elevated values of both biomarkers, suggesting a potential good response of this tumor to antiangiogenic drugs.

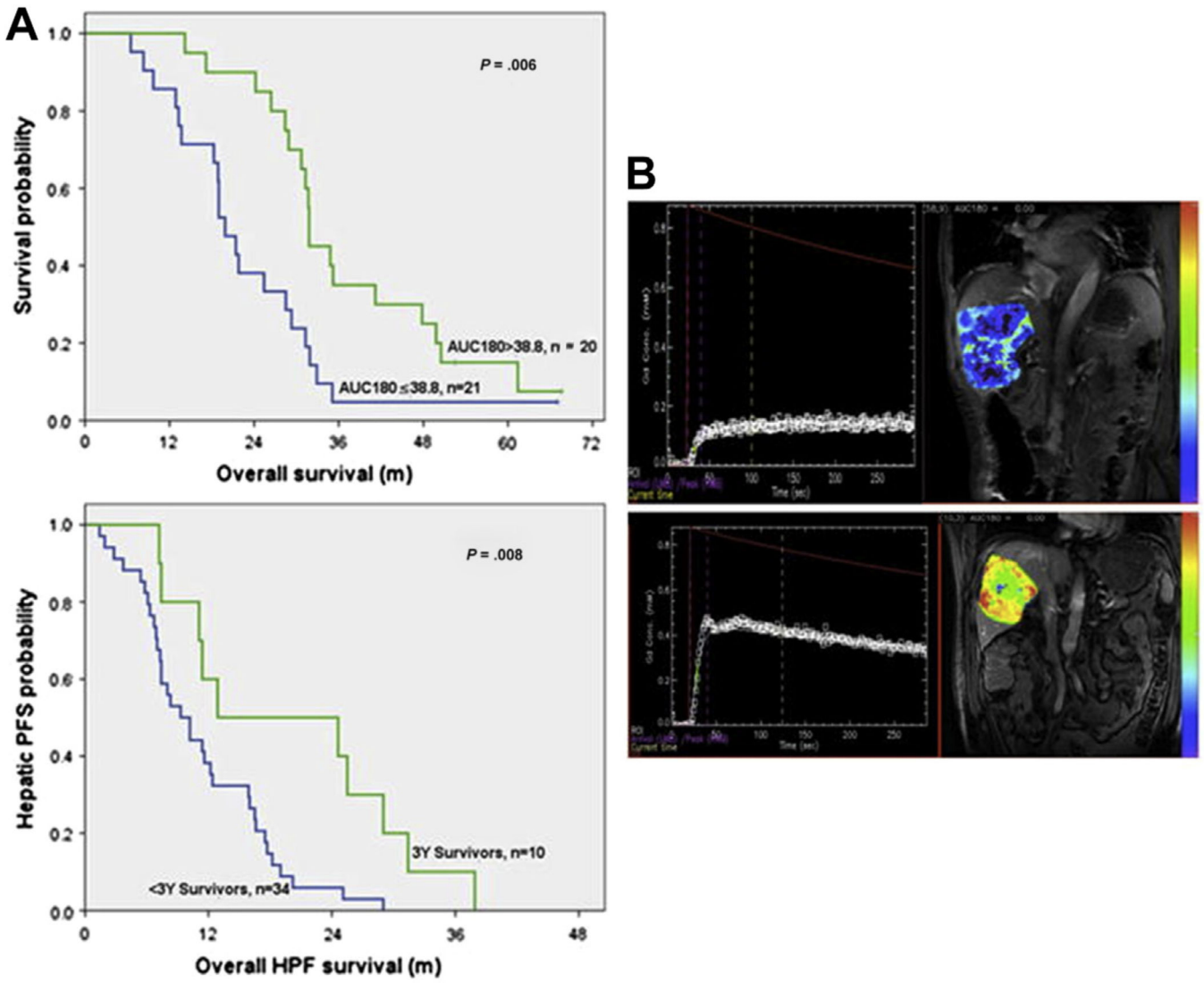

Fig. 16.

Perfusion parameters predict survival in patients with unresectable intrahepatic CHC: (*A*) Survival curves. Overall survival in patients with AUC 180 above or below the median value and hepatic progression free survival (HPF) in 3-year versus less than 3-year survivors. (*B*) Prechemotherapy DCE-MR imaging with low AUC curve of gadolinium and corresponding MR imaging show poor contrast enhancement in a less than 3-year survivor, and high AUC curve of gad-olinium and corresponding MR imaging showing greater contrast enhancement in a 3-year or greater survivor. PFS, progression-free survival. (*From* Konstantinidis IT, DoRKG, Gultekin DH, et al. Regional chemotherapy for unresectable intrahepatic cholangiocarcinoma: a potential role for dynamic magnetic resonance imaging as an imaging biomarker and a survival update from two prospective clinical trials. Ann Surg Oncol 2014;21(8):2675–83. with permission.)

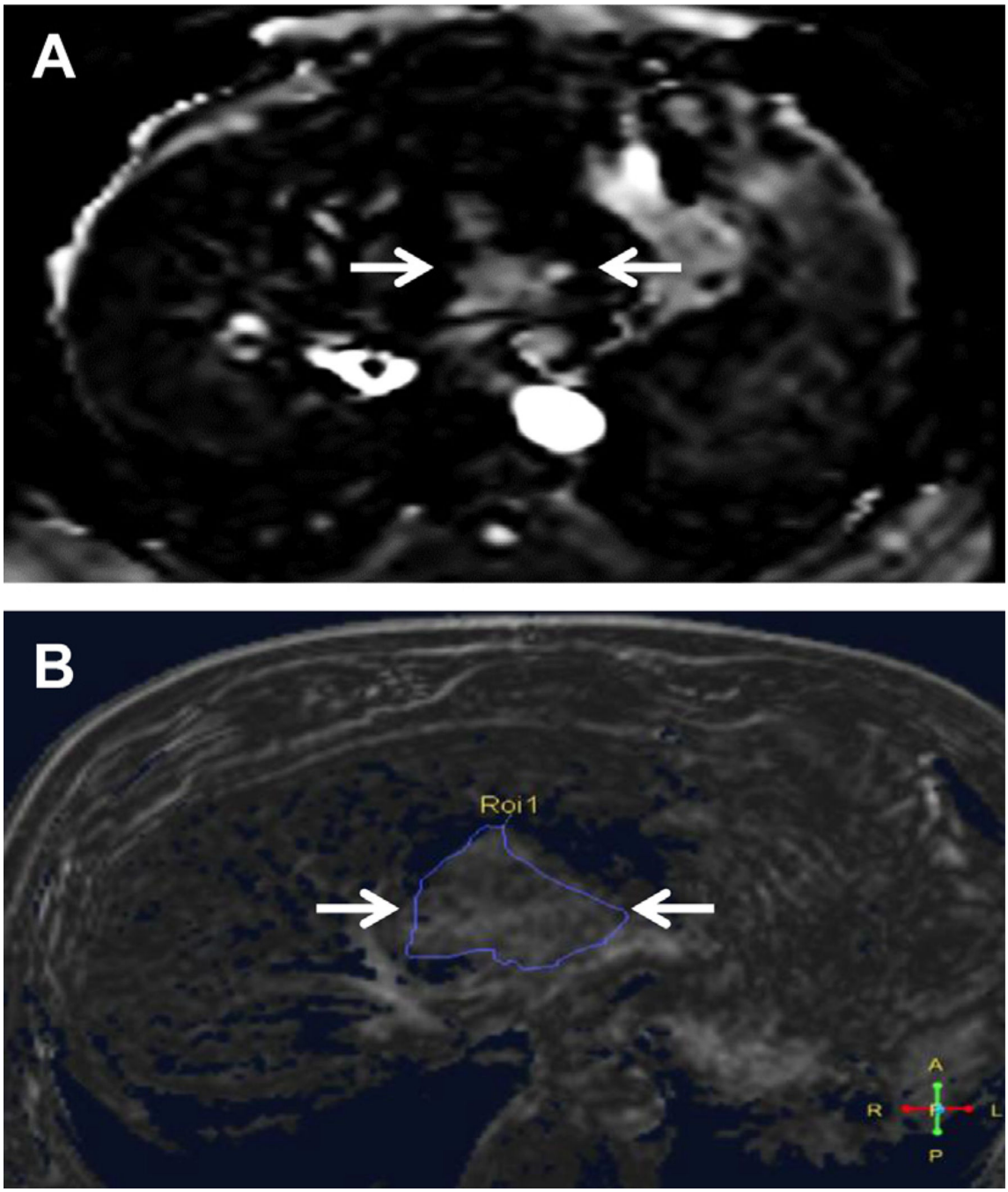

Fig. 17.

HCC (*arrows*) shows flow in the subtraction image of FAIR-ASL sequence (*A*) in a similar manner to the enhancement showed during the arterial phase (subtraction image) of a DCE-MR imaging sequence (*B*).

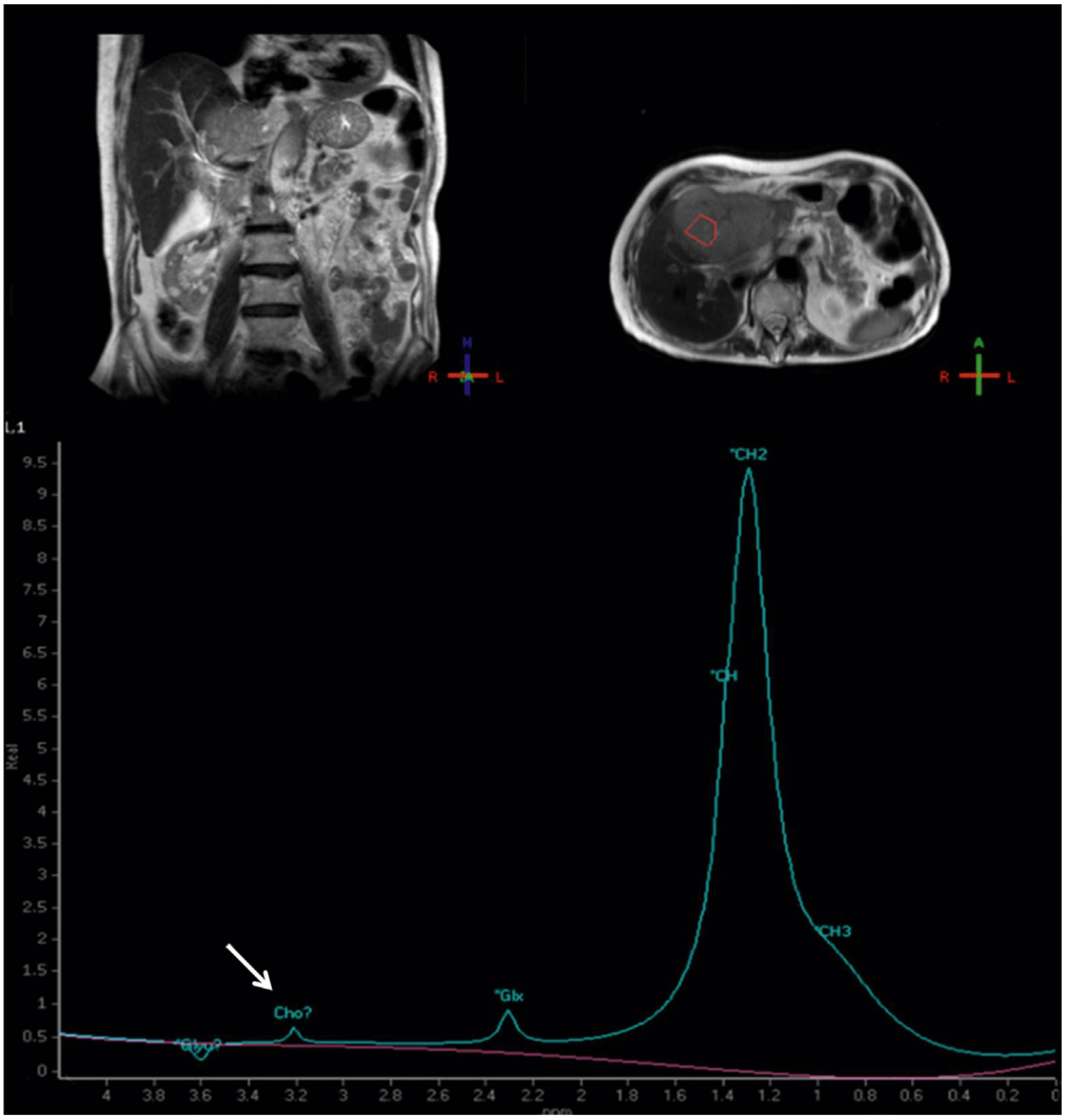

Fig. 18.

Assessment of well-differentiated HCC with single-voxel PRESS ^{1}H-MRS, which shows a peak of choline (Cho) at 3.2 ppm (*arrow*) and an increase of lipids (peak at 1.3 ppm), consistent with a malignant lesion.

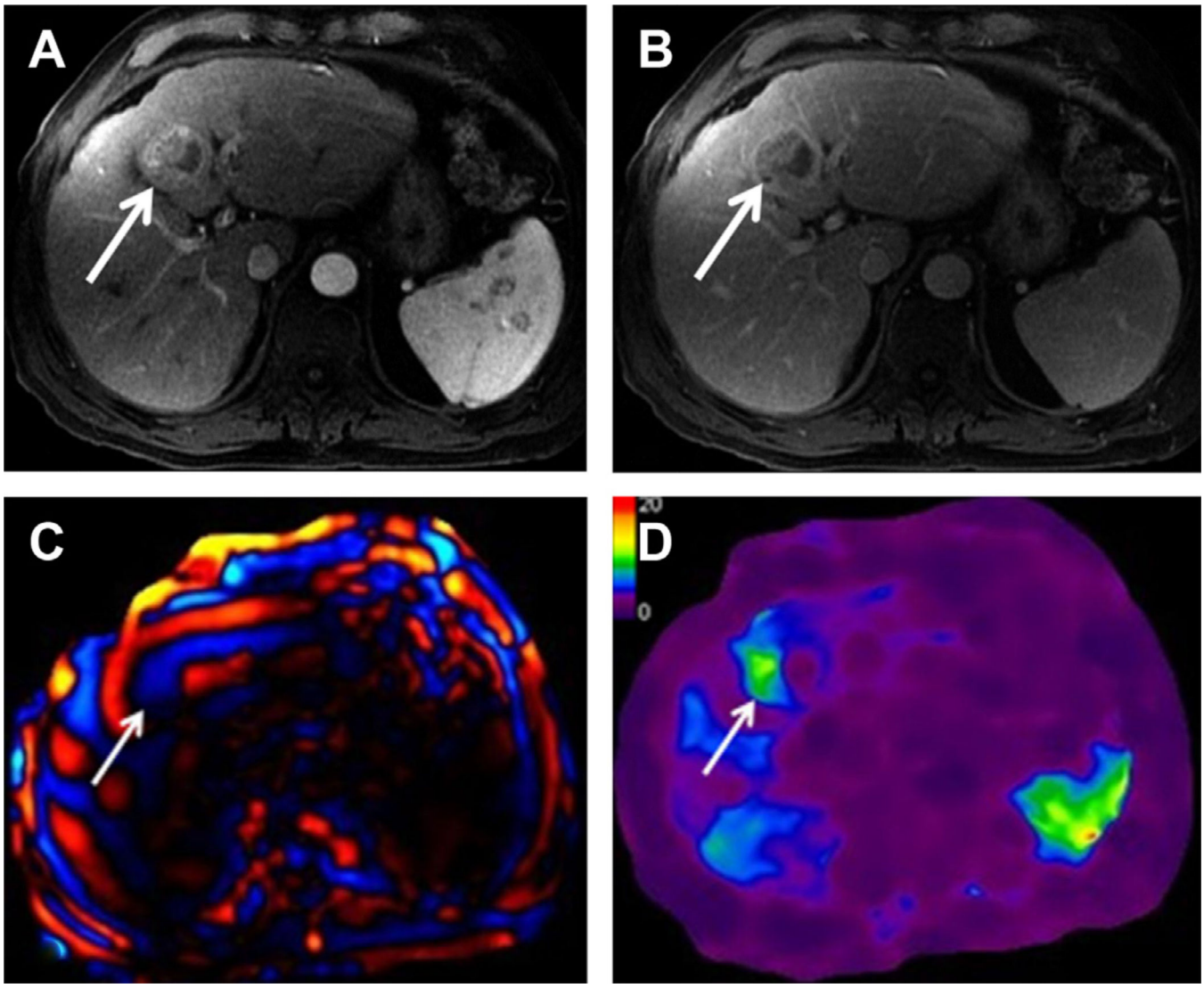

Fig. 19.

MRE of HCC (*arrows*). (*A, B*) DCE-MR imaging during the arterial and venous phases shows a nodule with the typical pattern of wash-in/washout. (*C, D*) Wave and elastogram maps demonstrate increased stiffness of the lesion with a value of 8.33 kPa, consistent with a malignant origin. (*Courtesy of* Alvin C. Silva, MD, Mayo Clinic, Scottdale, AZ.)

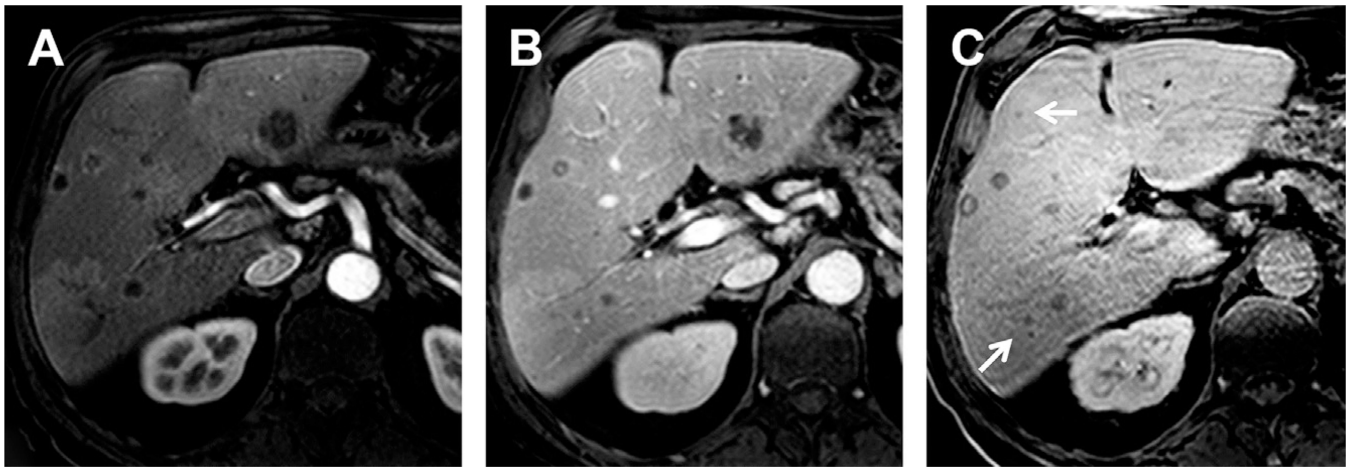

Fig. 20.

Pancreatic cancer liver metastasis with Gd-BOPTA. (*A, B*) DCE-MR imaging during arterial and venous phases demonstrates multiple nodules with ring enhancement. (*C*) The HB phase permits the depiction of more millimetric metastases (*arrows*), which appear as hypointense nodules.

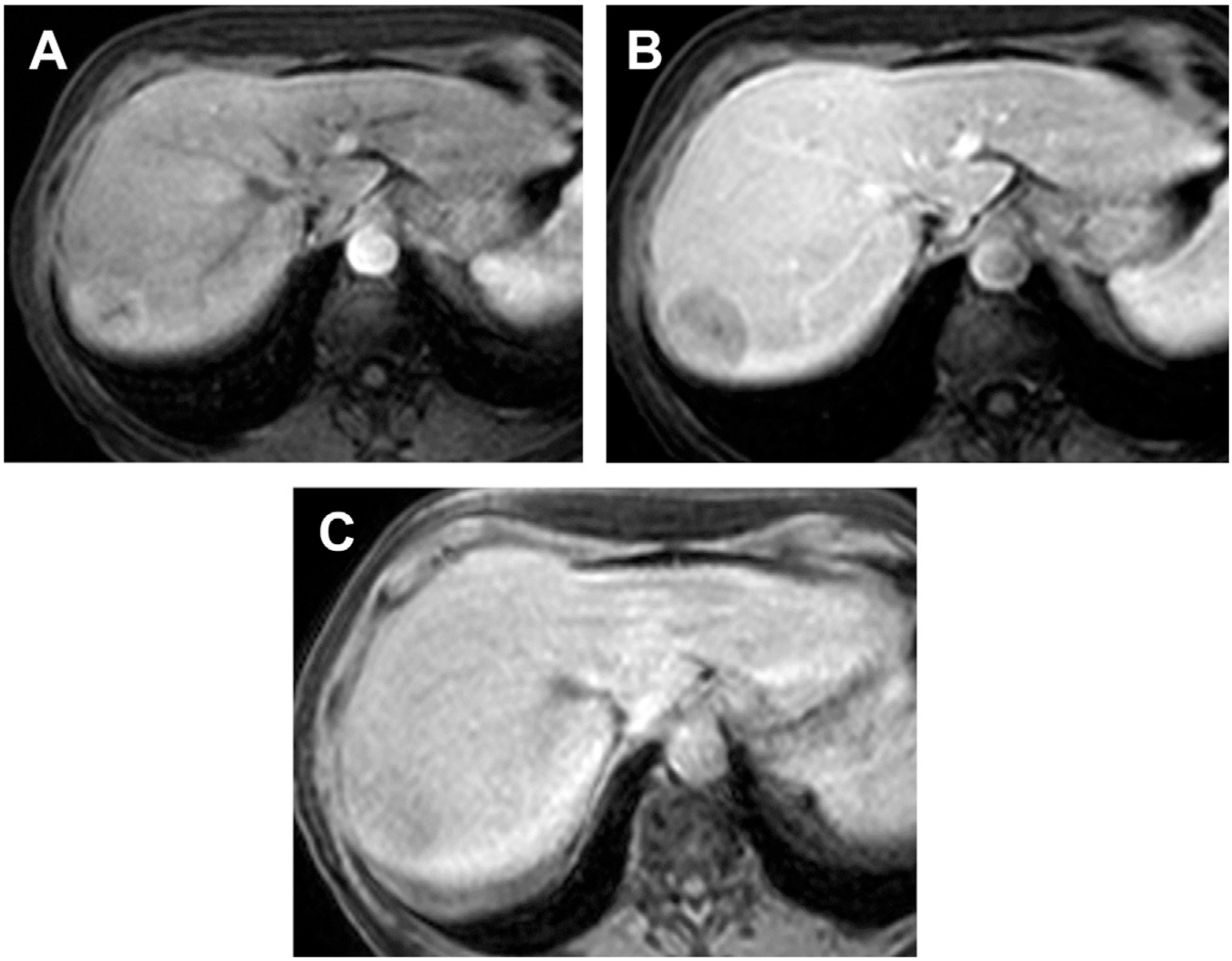

Fig. 21.

Well-differentiated HCC with Gd-BOPTA. (*A, B*) DCE-MR imaging during arterial and venous phases demonstrates a nodule with homogeneous enhancement on arterial phase and delayed washout (*C*) The nodule is slightly hypointense to liver parenchyma during the HB phase.

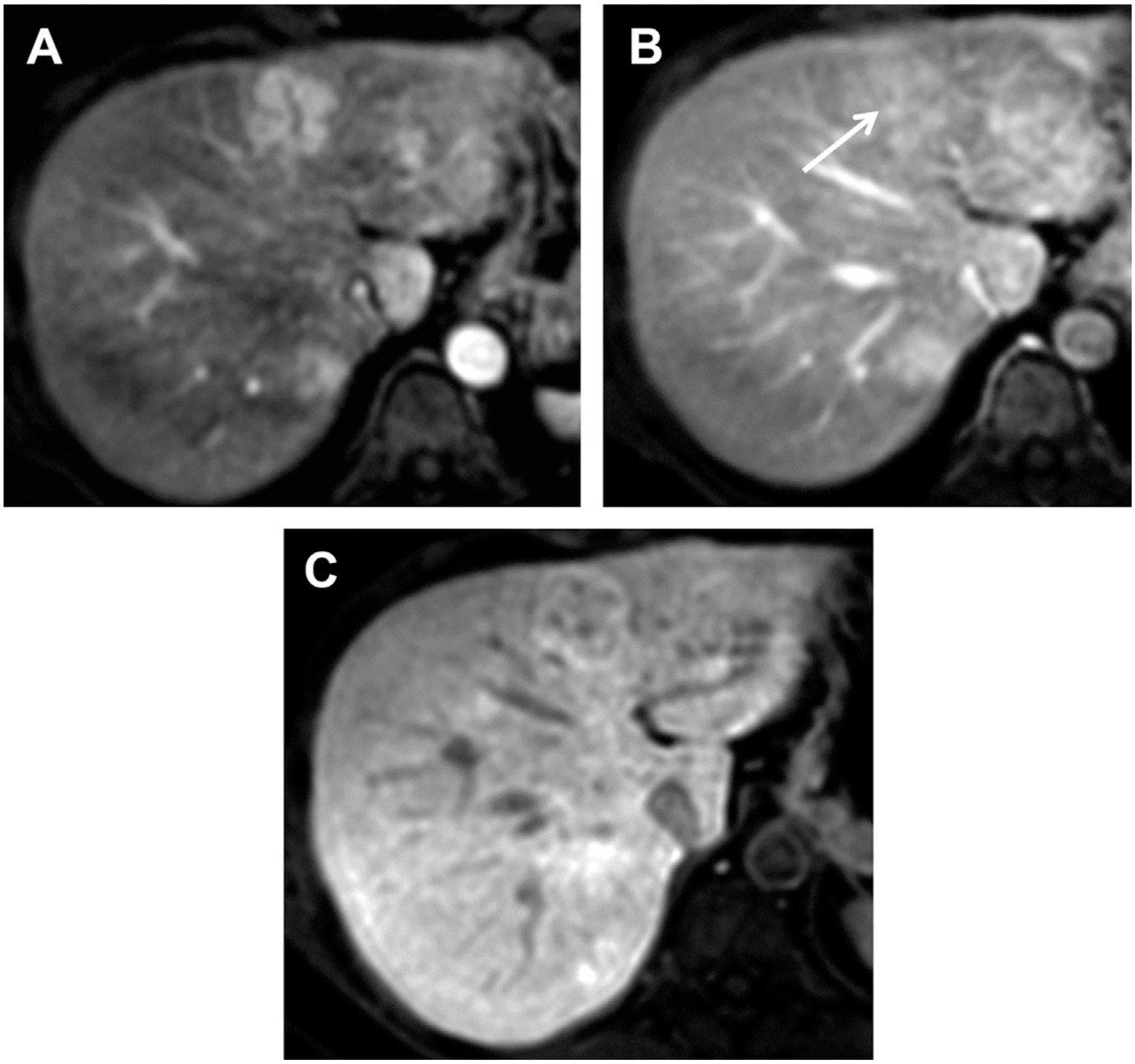

Fig. 22.

FNH with Gd-EOB-DTPA. (*A, B*) DCE-MR imaging during arterial and venous phases demonstrate a nodule with homogeneous enhancement on arterial phase, presenting a central hypovascular scar. The nodule becomes isointense to liver in the venous phase with enhancement of the scar (*arrow*). (*C*) Notice heterogeneous enhancement of the nodule during the HB phase.

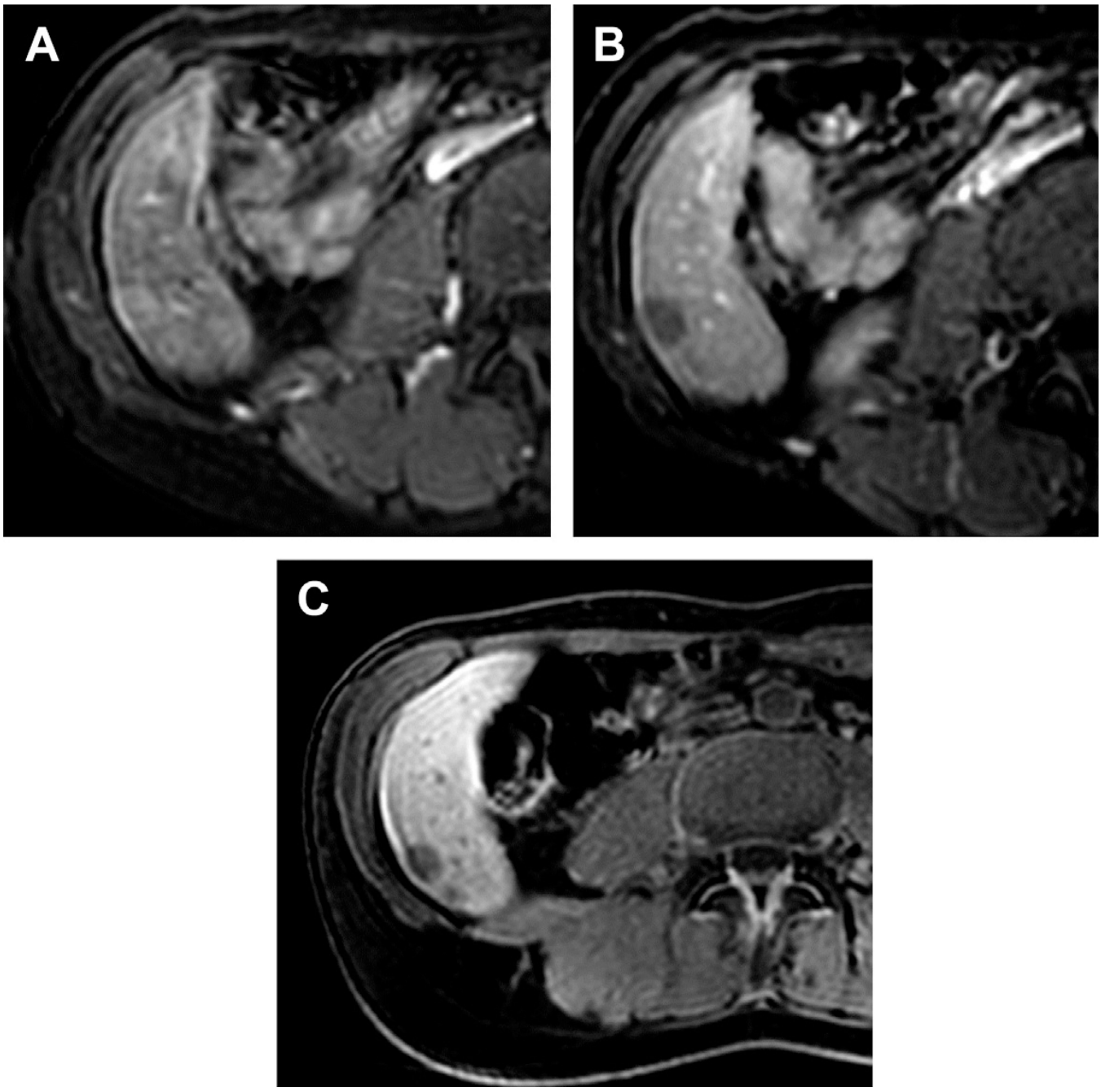

Fig. 23.

Hepatocellular adenoma with Gd-BOPTA. (*A, B*) DCE-MR imaging during arterial and venous phases demonstrate a nodule with enhancement on arterial phase and delayed washout. (*C*) Notice the absence of enhancement during the HB phase.

Table 1

MR imaging functional techniques for abdominal tumor evaluation

Tumor Feature	MR Imaging Technique	Quantitative Parameters
Cellularity, necrosis, and apoptosis	DWI	ADC
Metabolism	^{1}H-MRS	Ratio of choline (ppm) to other metabolites
Angiogenesis	DCE-MR imaging	K^{trans}, v_e, K_{ep}, V_p, AUC
Elasticity/stiffness	MRE	Young's modulus, shear modulus
Hepatic function	HB contrast agents	Lesion-to-liver enhancement ratio

Abbreviations: K_{ep}, rate constant; K^{trans}, efflux constant; v_e, volume of extravascular extracellular space; v_p, plasma volumen.

Table 2

Methods of analyzing a perfusion MR imaging examination of the abdomen

Method	Description	Advantage		Disadvantage	
Visual assessment	Images acquired in discrete breath-hold phases (early and/or late arterial, portal venous, and one or more delayed phases); enhancement patterns of the lesion and parenchyma analyzed by the radiologist	• No special technique required • Fairly accurate characterization of lesions		• Subjective • Intraobserver and interobserver variations • No quantitative parameters obtained, so difficult to follow-up lesions, assess treatment response after novel drug therapies	
Semiquantitative assessment	Change in SI over time is tracked	• Easy to use • Provides semiquantitative metrics of perfusion		• Actual contrast concentration not calculated, hence affected by factors as rate of contrast injection • Not a true reflection of the tissue perfusion and permeability	
Quantitative assessment	Change in concentration of GBCA with time is calculated; mathematic al models used to derive tissue perfusion and permeability paramete rs	• Tissue properties as blood flow, interstitial volume, and permeability are derived • Potentially more objective		• Complex postprocessing required • Not available on standard clinical scanners • No universally agreed on mathematical models to calculate perfusion parameters	

Table 3

Hepatobiliary contrast agents used for liver MR imaging

Generic Name	Abbreviated Name	Trade Name	Manufacturer
Gadobenate dimeglumine	Gd-BOPTA	Multihance	Bracco, Princeton, NJ, USA
Gadoxetic acid	Gd-EOB-DTPA	Eovist/Primovist	Bayer, Wayne, NJ, USA

Eovist is the trade name in the United States. Primovist is the trade name in the European Union, Australia, and Japan.

Table 4

Main characteristics of hepatobiliary contrast agents used for liver MR imaging

	Dosage (mMol/kg)	Injection Rate (mL/s)	Elimination	Dynamic Phase	Hepatospecific Phase	Maximum Biliary Excretion (mn)	NSF Association*
Gd-BOPTA	0.05	2–3	1%–2% liver 98% kidney	Same as extracellular contrast agents	60–240 mn Patient should be scanned twice Delayed in cirrhotic livers	40	No
Gd-EOB-DTPA	0.025	1–2	50% liver	Less SI on arterial phase	10–120 mn	10–20	No
			50% kidney	Overlap in venous and hepatospecific phase with limitations for hemangioma characteri zation	Delayed in cirrhotic livers		

Abbreviation: NSF, nephrogenic systemic fibrosis.

*No unconfounded cases of NSF after single-agent injection have been reported in peer-reviewed literature for any of both HBCAs. Recent data support the safety of Gd-BOPTA in patients with impaired renal function.[119,120]